

CONFIDENTIALCopy 5
RM A57K20

UNCLASSIFIED



RESEARCH MEMORANDUM

STATIC LONGITUDINAL AND LATERAL STABILITY AND CONTROL

CHARACTERISTICS OF A MODEL OF A SWEEP-WING FIGHTER-

BOMBER TYPE AIRPLANE WITH A TOP INLET AT MACH

NUMBERS FROM 1.6 TO 2.35

By A. Vernon Gnos and Richard L. Kurkowski

Ames Aeronautical Laboratory
Moffett Field, Calif.

CLASSIFICATION CHANGED

UNCLASSIFIED

By *TPA #46*
Date *2/4/58*

To
By authority

CLASSIFIED DOCUMENT

This material contains information affecting the National Defense of the United States within the meaning of the Espionage Laws, Title 18, U.S.C., Secs. 793 and 794, the transmission or revelation of which in any manner to an unauthorized person is prohibited by law.

NATIONAL ADVISORY COMMITTEE FOR AERONAUTICS

WASHINGTON

March 3, 1958

CONFIDENTIAL**LIBRARY COPY**

MAR 5 1958

LANGLEY AERONAUTICAL LABORATORY
LIBRARY, NACA
LANGLEY FIELD, VIRGINIA



NATIONAL ADVISORY COMMITTEE FOR AERONAUTICS

UNCLASSIFIED

RESEARCH MEMORANDUM

STATIC LONGITUDINAL AND LATERAL STABILITY AND CONTROL

CHARACTERISTICS OF A MODEL OF A SWEEP-WING FIGHTER-

BOMBER-TYPE AIRPLANE WITH A TOP INLET AT MACH

NUMBERS FROM 1.6 TO 2.35

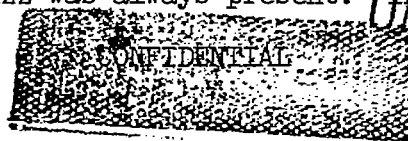
By A. Vernon Gnos and Richard L. Kurkowski

SUMMARY

Static longitudinal and lateral stability characteristics of a swept-wing fighter-bomber airplane model with a top inlet have been determined experimentally. In addition, vertical-tail effectiveness, spoiler effectiveness, effects of several store configurations, and effects of mass flow were investigated. Tests were made at Mach numbers of 1.6, 1.8, 2.0, 2.2, and 2.35 and Reynolds numbers, based upon mean aerodynamic chord, of between 2.0×10^6 and 2.5×10^6 .

INTRODUCTION

A swept-wing fighter-bomber-type airplane model with a top inlet was the subject of an investigation in the Ames 9- by 7-foot supersonic wind tunnel (ref. 1). The engine air inlet of the test configuration was located on the top of the fuselage behind the cockpit canopy. This unusual inlet location has a number of advantages both aerodynamic and mechanical. Some of the more important advantages that accrue from this location include: freedom for carrying stores under the fuselage, short duct lines, and the possibility of good high angle-of-attack characteristics. Since inlet location can have important effects upon stability characteristics of an airplane, especially where the inlet is large, the subject investigation of the top-inlet model was conducted. Further, because the vertical tail and parts of the fuselage are immersed in the external flow field of the inlet, variation of internal flow conditions can affect the lateral characteristics of the airplane. Accordingly, the investigation included the effect on lateral characteristics of three mass-flow conditions: supercritical, engine matched (approximate), and low subcritical where buzz was always present. In addition, the effects



UNCLASSIFIED

of store configuration upon longitudinal and lateral characteristics and the effects of spoiler deflection upon lateral control power were investigated.

NOTATION

Force and moment coefficients are referred to the stability axes with the origin on the fuselage reference axis at the projection of the 35-percent point of the wing mean aerodynamic chord. The system of axes and the positive direction of forces, moments, and angles are shown in figure 1.

C_D drag coefficient, $\frac{\text{measured drag} - \text{base drag} - \text{internal drag}}{qS}$

C_L lift coefficient, $\frac{\text{lift}}{qS}$

C_Y side-force coefficient, $\frac{\text{side force}}{qS}$

C_l rolling-moment coefficient, $\frac{\text{rolling moment}}{qSb}$

C_m pitching-moment coefficient, $\frac{\text{pitching moment}}{qS\bar{c}}$

C_n yawing-moment coefficient, $\frac{\text{yawing moment}}{qSb}$

M free-stream Mach number

S basic wing area, 3.046 sq ft

b wing span, 3.292 ft

c wing chord, ft

\bar{c} wing mean aerodynamic chord, M.A.C., 1.019 ft

q free-stream dynamic pressure, lb/sq ft

$\frac{m_s}{m_\infty}$ mass-flow ratio, $\frac{\text{compressor mass flow}}{\text{free-stream mass flow based on capture area}}$

α angle of attack, deg

β	angle of sideslip, deg
δ_{d1}	angular deflection of inboard deflector, deg
δ_{d2}	angular deflection of intermediate inboard deflector, deg
δ_{d3}	angular deflection of intermediate outboard deflector, deg
δ_{d4}	angular deflection of outboard deflector, deg
δ_{s1}	angular deflection of inboard spoiler, deg
δ_{s2}	angular deflection of intermediate inboard spoiler, deg
δ_{s3}	angular deflection of intermediate outboard spoiler, deg
δ_{s4}	angular deflection of outboard spoiler, deg
δ_v	angular deflection of vertical tail, deg
$C_{l\beta}$	rate of change of rolling-moment coefficient with sideslip angle, $\frac{\partial C_l}{\partial \beta}$, per deg
$C_{n\beta}$	rate of change of yawing-moment coefficient with sideslip angle, $\frac{\partial C_n}{\partial \beta}$, per deg

MODEL

The model is illustrated in the photographs of figure 2. Sketches of configuration details are shown in figure 3. Geometric dimensions are listed in table I.

The test model was mounted on a hollow sting by a seven-component strain-gage balance so that forces and moments were recorded simultaneously with the internal-flow measurements. The balance consisted of four normal-force gages, two side-force gages, and a chord-force gage.

Balance forces were read out and recorded by conventional wind-tunnel equipment. The model had a vertical-wedge inlet, subsonic diffuser, wedge boundary-layer bleed system, fuselage boundary-layer bleed system, and cooling and ventilating intake scoops and exit. Internal flow was regulated with an iris valve located at the exit of the hollow sting. Mass flow was measured with a calibrated flow meter which was built into the sting.

Three store configurations were tested with the model. They included a semisubmerged tank without fins as shown in figure 3(a), a saddle tank, and a saddle tank plus small store with fins as shown in figure 3(b).

The model was provided with an all-movable vertical tail which was tested at deflection angles of 0° and -3° and an all-movable horizontal tail which was tested with no deflection.

The left wing of the model was provided with an instrumented spoiler-slot-deflector system. Each spoiler and deflector could be adjusted to fixed deflection angles of between 5° and 70° . Spoiler details are shown in figures 2(c), 2(d), 3(a), and 3(c). The spoilers and deflectors were replaced with blank plates for tests which required no spoiler deflection.

TEST PROCEDURE

The investigation was conducted at Mach numbers of 1.6, 1.8, 2.0, 2.2, and 2.35 and Reynolds numbers based upon mean aerodynamic chord of between 2.0×10^6 and 2.5×10^6 . Angle of attack was varied from -6° to $+20^\circ$ and angle of sideslip was varied from -9° to $+4^\circ$. Sideslip runs were made at nominal angles of attack of -5° , 0° , 7° , and 14° . Mass-flow ratio was set at the estimated matched value for the model attitude of 2° angle of attack and 0° sideslip. No further adjustment of the mass flow was made during pitch or sideslip runs, even though "buzz" (defined as unsteady flow in the inlet and subsonic diffuser at subcritical mass-flow conditions) was sometimes encountered. Buzz generally occurred above 4° sideslip at a Mach number of 1.8 and above 2° sideslip at a Mach number of 2.2. Buzz was not encountered during pitch runs.

Measured angles of attack and sideslip were corrected for the tunnel stream angle and for sting and balance deflection under load. A buoyancy correction was applied to take into account tunnel static-pressure variations. The data have been corrected by adjusting the measured base pressure to free-stream static pressure. In addition the internal drag, which was determined from the change in momentum from free-stream conditions to measured conditions at the duct exit, was subtracted from measured drag. No corrections were made for inlet spillage drag or for internal drag of the cockpit cooling and ventilating air flow. Deflections of the vertical tail, spoilers, and deflectors under load were not known.

Precision of the data, which was determined from scatter and repeatability for moderate angle-of-attack conditions, is indicated in the following table:

C_D	± 0.0005
C_L	± 0.01
C_Y	± 0.002
C_z	± 0.0005
C_m	± 0.002
C_n	± 0.0005
M	± 0.005
m_3/m_∞	± 0.005
α , deg	± 0.1
β , deg	± 0.1

RESULTS

The longitudinal characteristics of the basic configuration and the tail off configuration are presented in figure 4. In figure 5 longitudinal characteristics with two additional store configurations are shown. Figure 6 summarizes pitching moment at zero lift and aerodynamic center location as taken from figures 4 and 5.

Angle-of-attack effects on lateral characteristics of the basic configuration are shown in figure 7 and summarized in figure 8. Angle-of-attack effects on lateral characteristics of the vertical tail off configuration are presented in figure 9 and summarized in figure 10. Figure 11 presents the effect of vertical tail on lateral characteristics of the basic configuration. The effect of vertical tail on the lateral characteristics of the saddle tank and store configuration is presented in figure 12.

The effect at Mach number 2.2 of internal flow conditions upon lateral characteristics of the basic configuration is shown in figure 13 and of the vertical tail off configuration is shown in figure 14.

Rolling-moment effects of spoiler deflection are presented in figure 15. Figure 16 presents yawing-moment effects of spoiler deflection. In figure 17 the effect of spoiler deflection on longitudinal characteristics is shown.

SUMMARY OF RESULTS

General observations regarding the results are as follows:

1. Aerodynamic center did not shift significantly with Mach number for any of the tail-on configurations. Store configuration had little effect upon the location of the aerodynamic center.
2. Directional stability was maintained to about 12° angle of attack at a Mach number of 2.2. The usual trend of a decrease in directional stability with an increase in either angle of attack or Mach number was evident.
3. Large changes in directional stability were encountered at low inlet mass-flow ratios at a Mach number of 2.2. The vertical-tail contribution to directional stability was not seriously affected by low inlet mass-flow conditions since similar changes were obtained with the tail off. There were shifts in directional stability near 0° angle of sideslip associated with unstable air flow in the twin-duct system at low inlet mass flows.

Ames Aeronautical Laboratory
National Advisory Committee for Aeronautics
Moffett Field, Calif., Nov. 20, 1957

REFERENCE

1. Huntsberger, Ralph F., and Parsons, John F.: The Design of Large High-Speed Wind Tunnels. Papers presented at 5th meeting of Wind Tunnel and Model Testing Panel, AGARD, Fourth General Assembly, Scheveningen, The Netherlands, Rep. AG 15/P6, May 3-7, 1954, pp. 127-152.

TABLE I.- GEOMETRIC CHARACTERISTICS OF MODEL

Wing	
Total basic area, sq in.	438.6
Span, in.	39.51
Aspect ratio	3.56
Taper ratio	0.300
Dihedral angle, deg	0
Root chord, in.	17.13
Tip chord (equivalent), in.	5.22
Mean aerodynamic chord, in.	12.23
Wing station of mean geometric chord, in.	8.07
Sweepback of quarter chord, deg	45.0
Incidence, deg	0
Thickness, percent	5
Airfoil section	NACA 66005 modified
Fuselage	
Length, in.	58.70
Vertical tail	
Total area, sq in.	98.21
Span, in.	11.78
Aspect ratio	1.49
Taper ratio	0.301
Root chord, in.	12.18
Tip chord (equivalent), in.	3.68
Mean aerodynamic chord, in.	8.69
Sweepback of quarter chord, deg	45.0
Ratio of vertical-tail area to wing area	0.224
Area moment, cu in.	853.5
Thickness, percent	3.5
Airfoil section	NACA 65A003.5
Horizontal tail	
Total area, sq in.	115.31
Span, in.	20.22
Aspect ratio	3.54
Taper ratio	0.302
Dihedral, deg	0
Root chord, in.	8.79
Tip chord (equivalent), in.	2.69
Mean aerodynamic chord, in.	6.28
Sweepback of quarter chord, deg	45.0
Ratio of horizontal-tail area to wing area	0.263
Thickness, percent	3.5
Airfoil section	NACA 65A003.5

TABLE I.- GEOMETRIC CHARACTERISTICS OF MODEL - Concluded

Horizontal stabilizer	
Area (movable portion only), sq in.	76.65
Span, total (movable portion only), in.	15.29
Area moment, cu in.	352.7
Trailing-edge angle, deg	4.63
Semisubmerged tank	
Plan-form area, sq in.	48.17
Length, in.	22.95
Maximum diameter, in.	2.97
Leading-edge location (fuselage station), in.	26.28
Small center-line store and saddle tank	
Saddle tank length	23.31
Saddle tank leading-edge location (fuselage station), in. .	26.28
Store length, in.	15.30
Store maximum diameter, in.	1.80
Store leading-edge location (fuselage station), in.	28.71

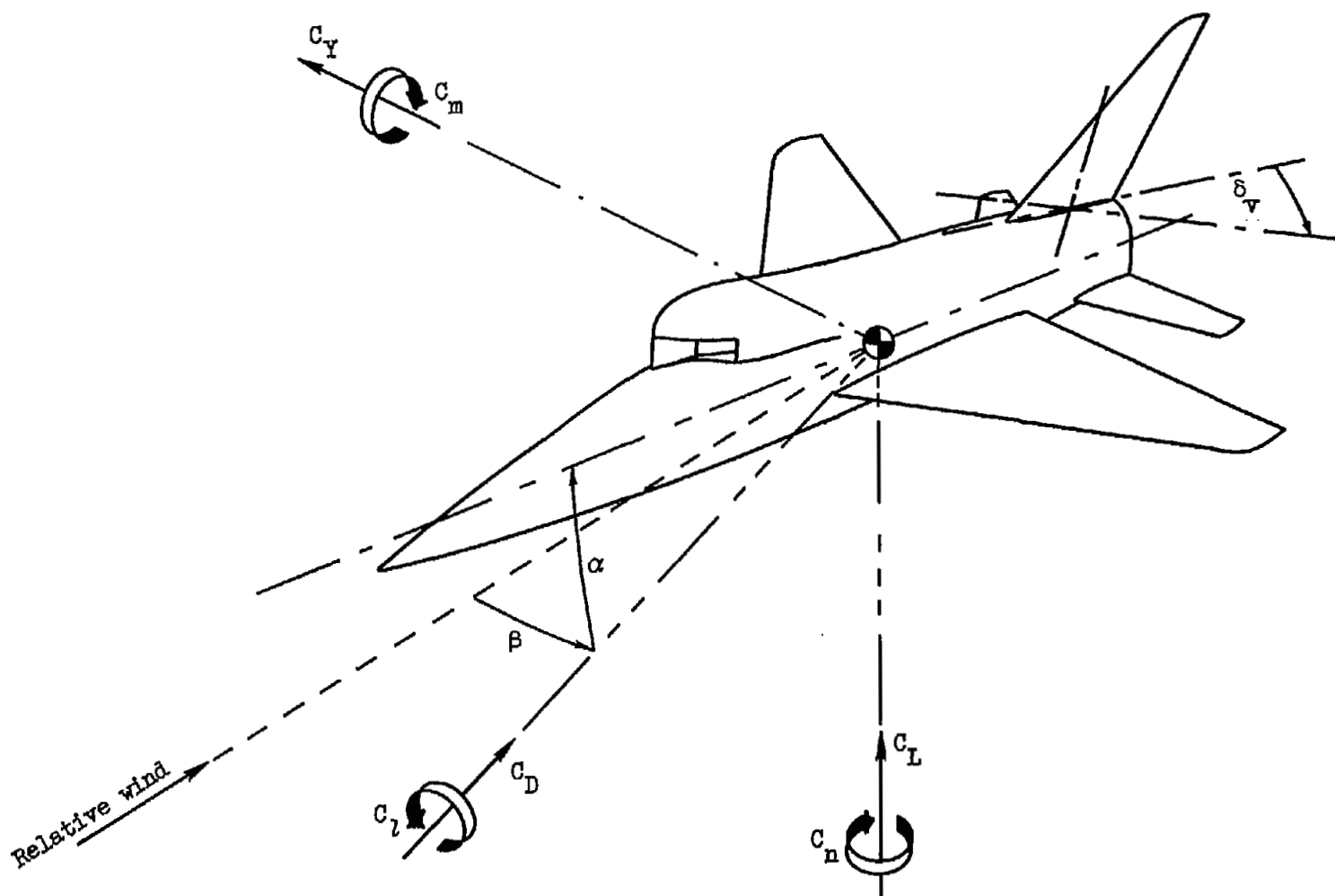
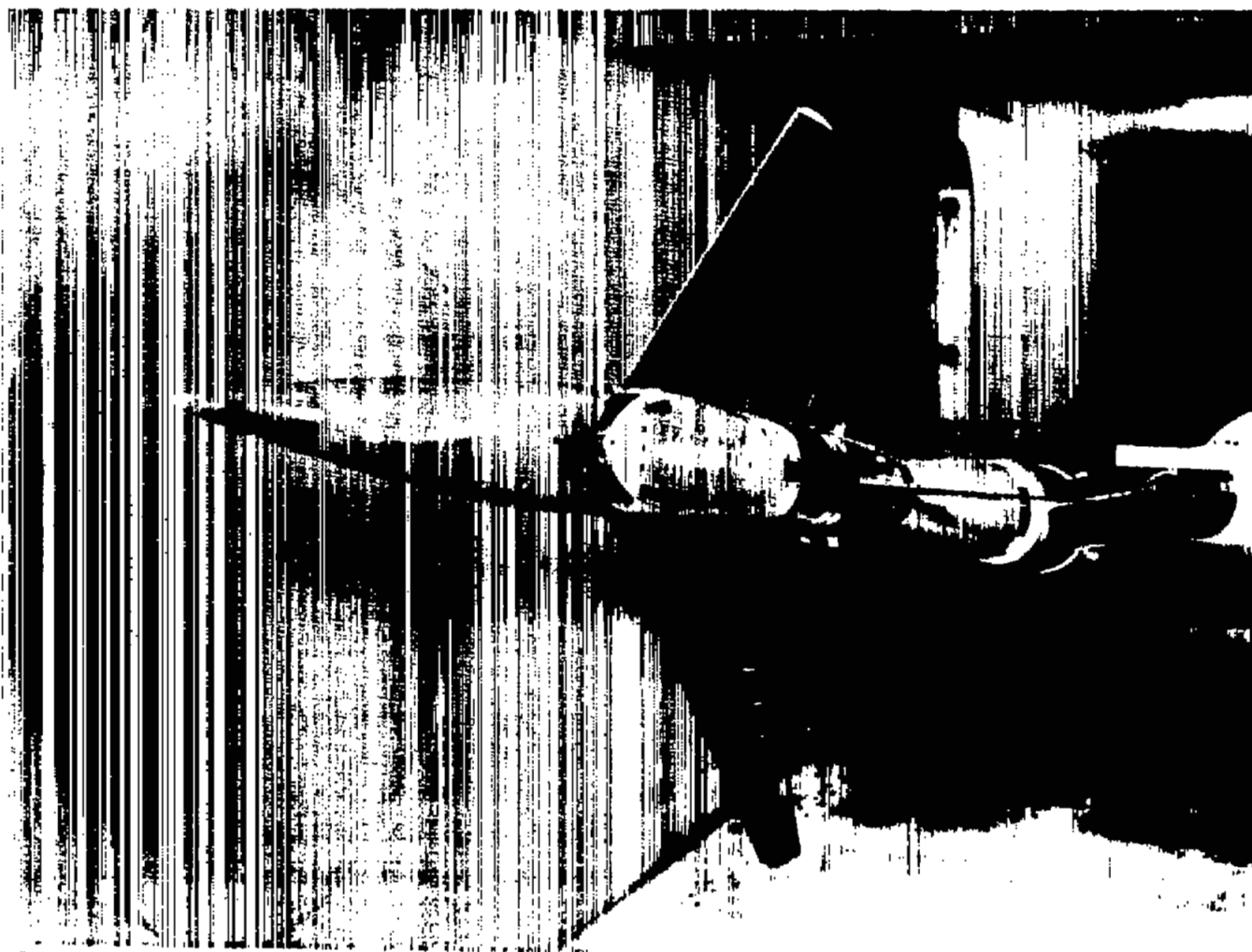


Figure 1.- System of axes and positive direction of forces, moments, and angles.



(a) Three-quarter top view of basic configuration with spoilers deflected 70° .

A-22427

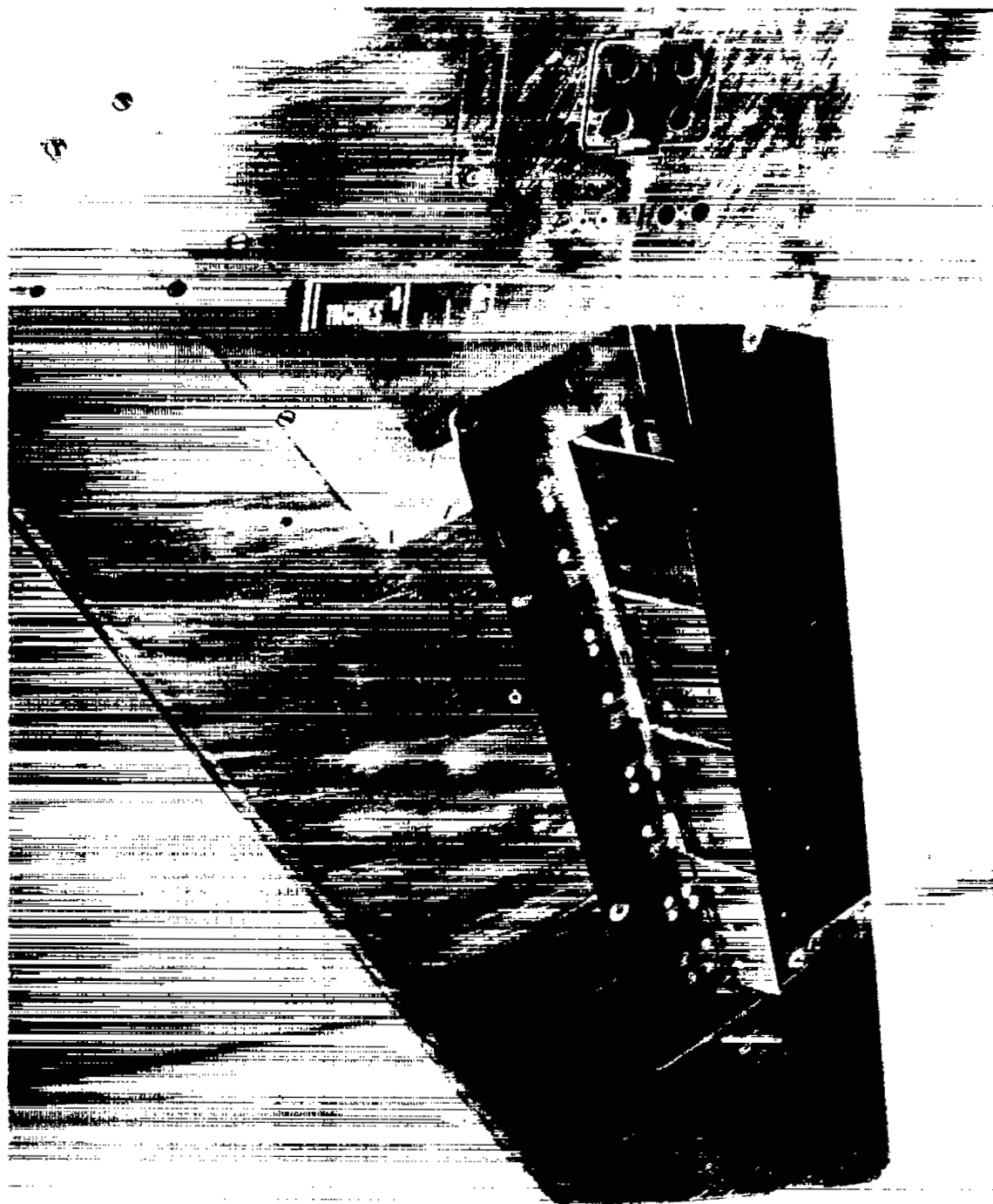
Figure 2.- Model photographs.



A-22429

(b) Three-quarter bottom view of basic configuration with deflectors deflected 70° .

Figure 2.- Continued.



(c) Close-up of spoiler detail.

A-22428

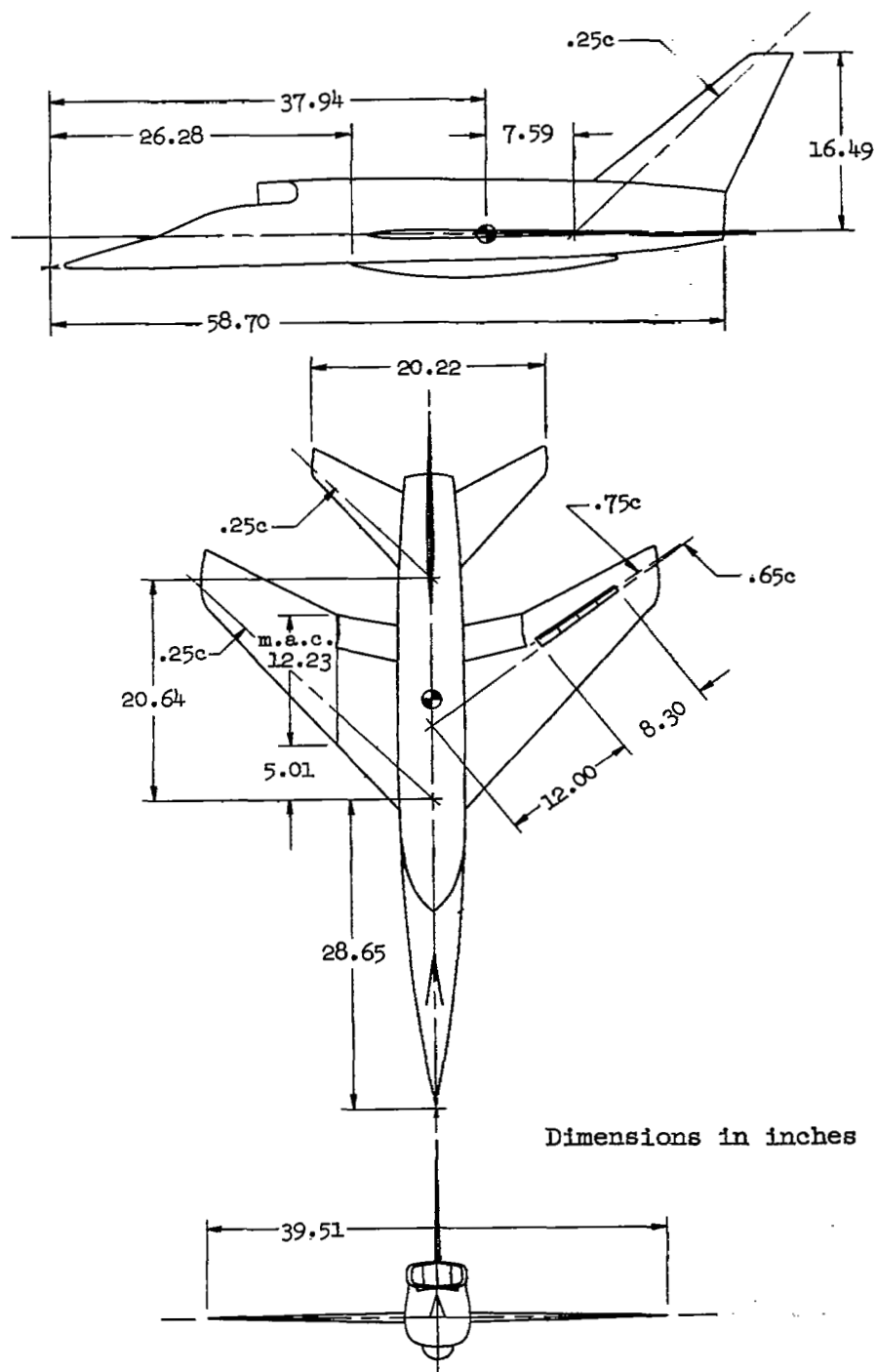
Figure 2.- Continued.



(d) Close-up of deflector details.

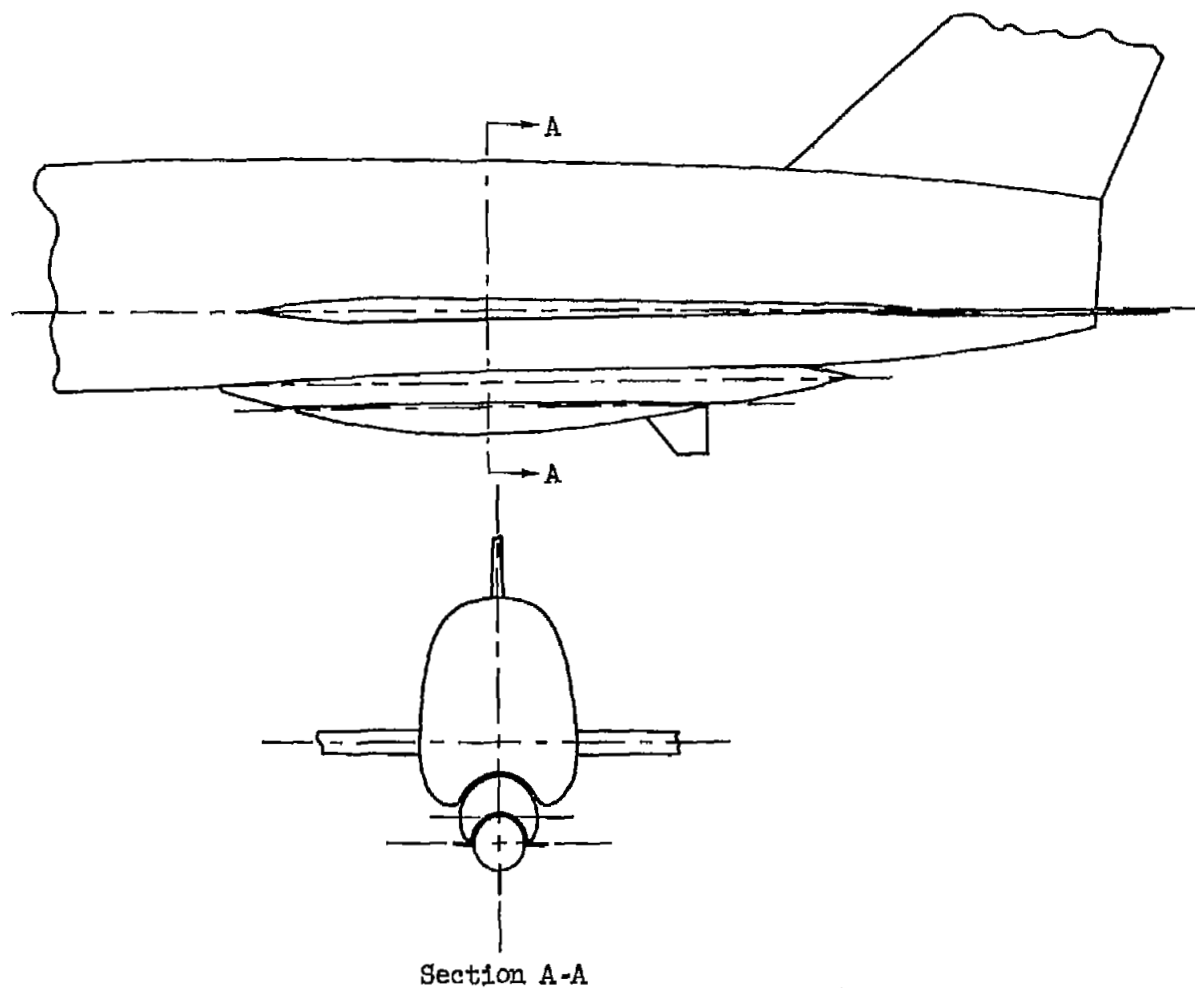
A-22430

Figure 2.- Concluded.



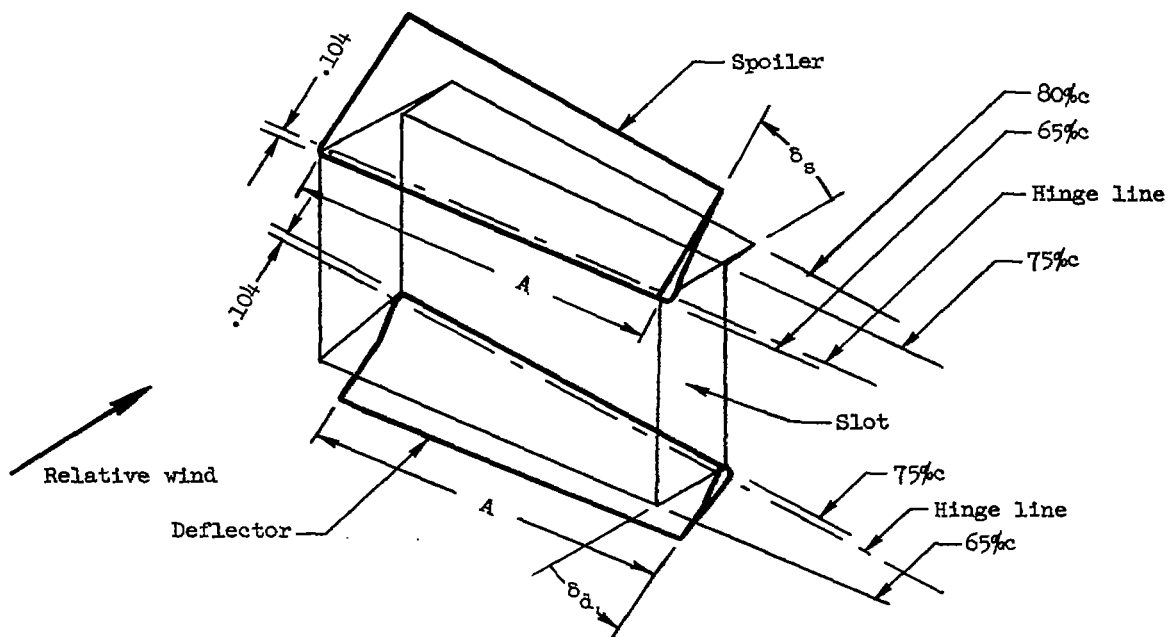
(a) Three views of basic configuration with spoiler-slot-deflector system.

Figure 3.- Configuration details.



(b) Saddle-tank and store arrangement.

Figure 3.- Continued.



Spoiler-slot-deflector dimensions

	Chord		Length	Plan form ²
	% c	mean, in. ¹	A, in.	sq in.
Spoiler No. 1	15	1.25	2.04	2.55
Spoiler No. 2	15	1.12	1.98	2.22
Spoiler No. 3	15	1.00	1.99	1.99
Spoiler No. 4	15	0.88	2.04	1.79
Slot	10	1.06	8.05	8.53
Deflector No. 1	10	0.78	2.04	1.59
Deflector No. 2	10	0.70	1.98	1.38
Deflector No. 3	10	0.62	1.99	1.23
Deflector No. 4	10	0.54	2.04	1.10

- 1 Mean chord - measured perpendicular to the hinge line from the hinge line to the opposite edge
- 2 Plan form - length A times the mean chord

(c) Spoiler-slot-deflector system, dimensions, and direction of deflections.

Figure 3.- Concluded.

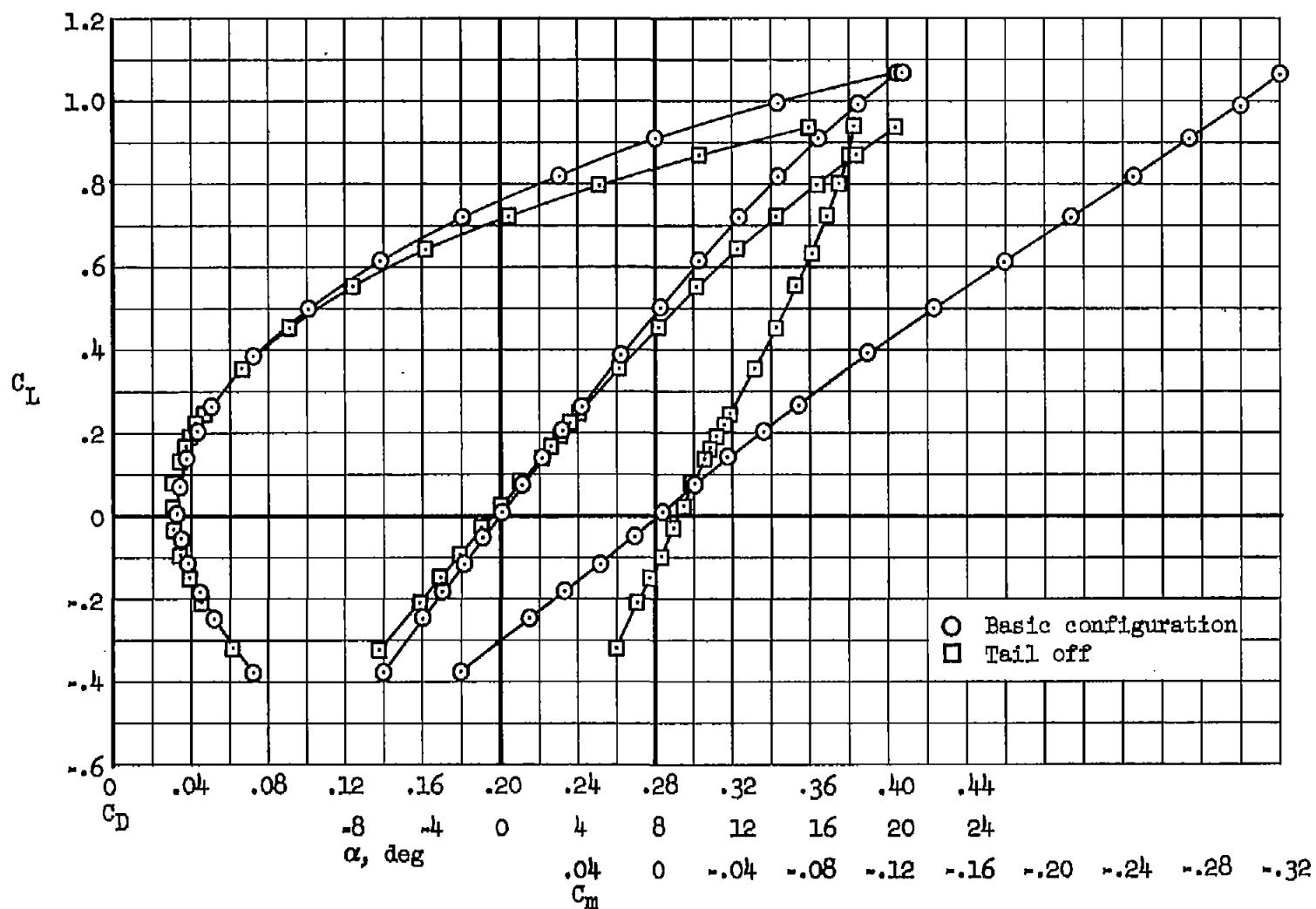
(a) $M = 1.6$

Figure 4.- Effect of horizontal tail on longitudinal characteristics.

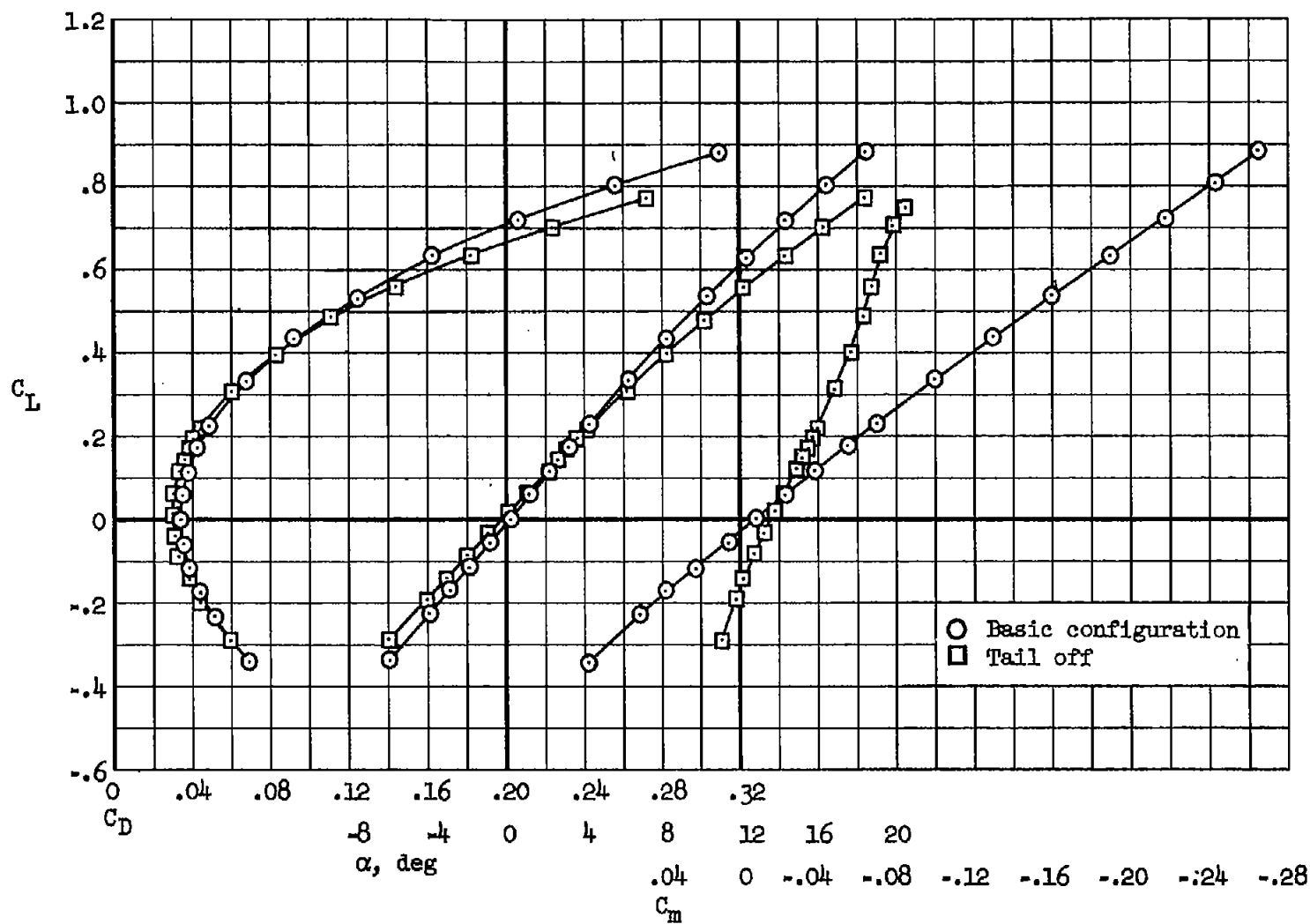
(b) $M = 1.8$

Figure 4.- Continued.

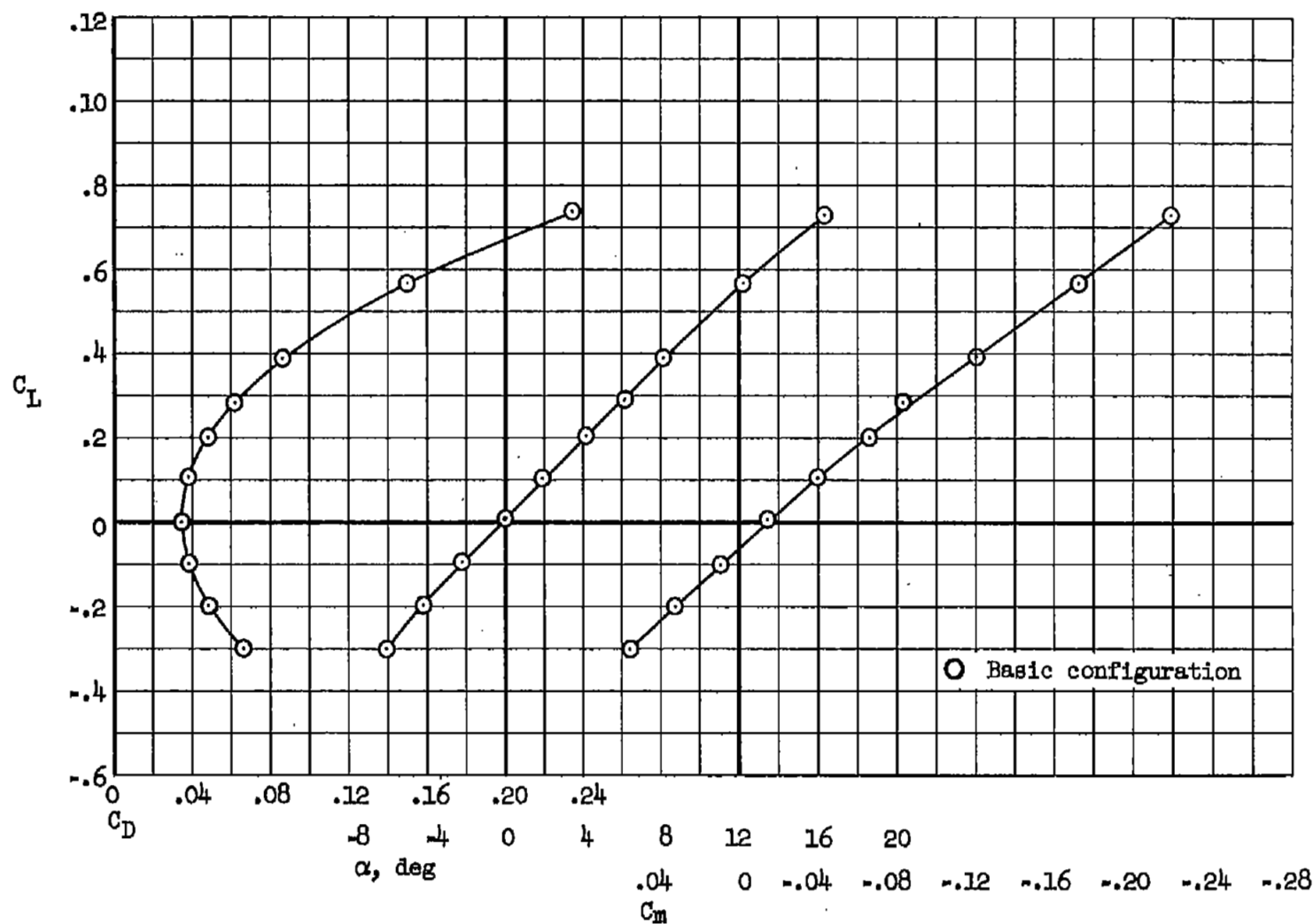
(c) $M = 2.0$

Figure 4.- Continued.

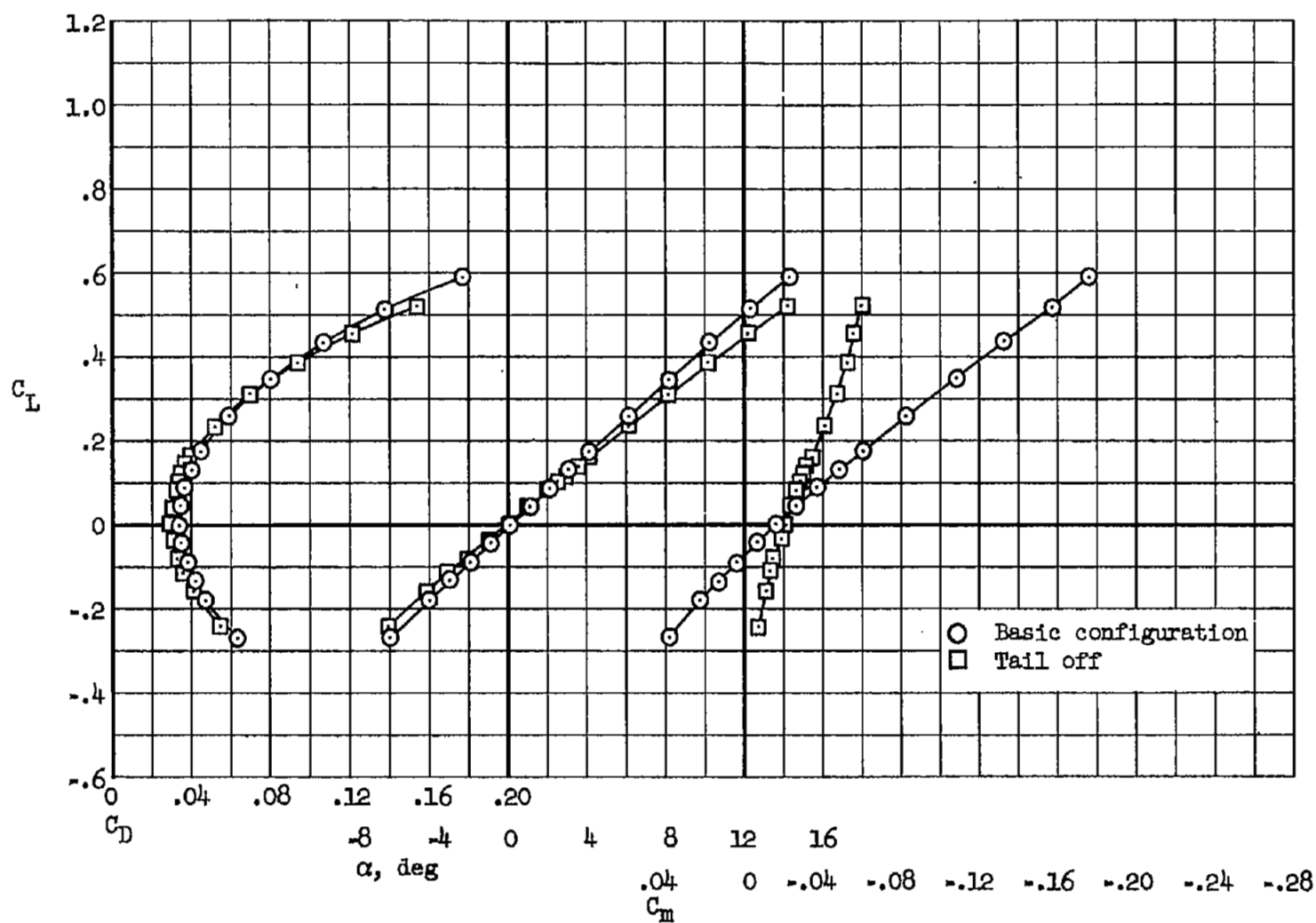
(d) $M = 2.2$

Figure 4.- Continued.

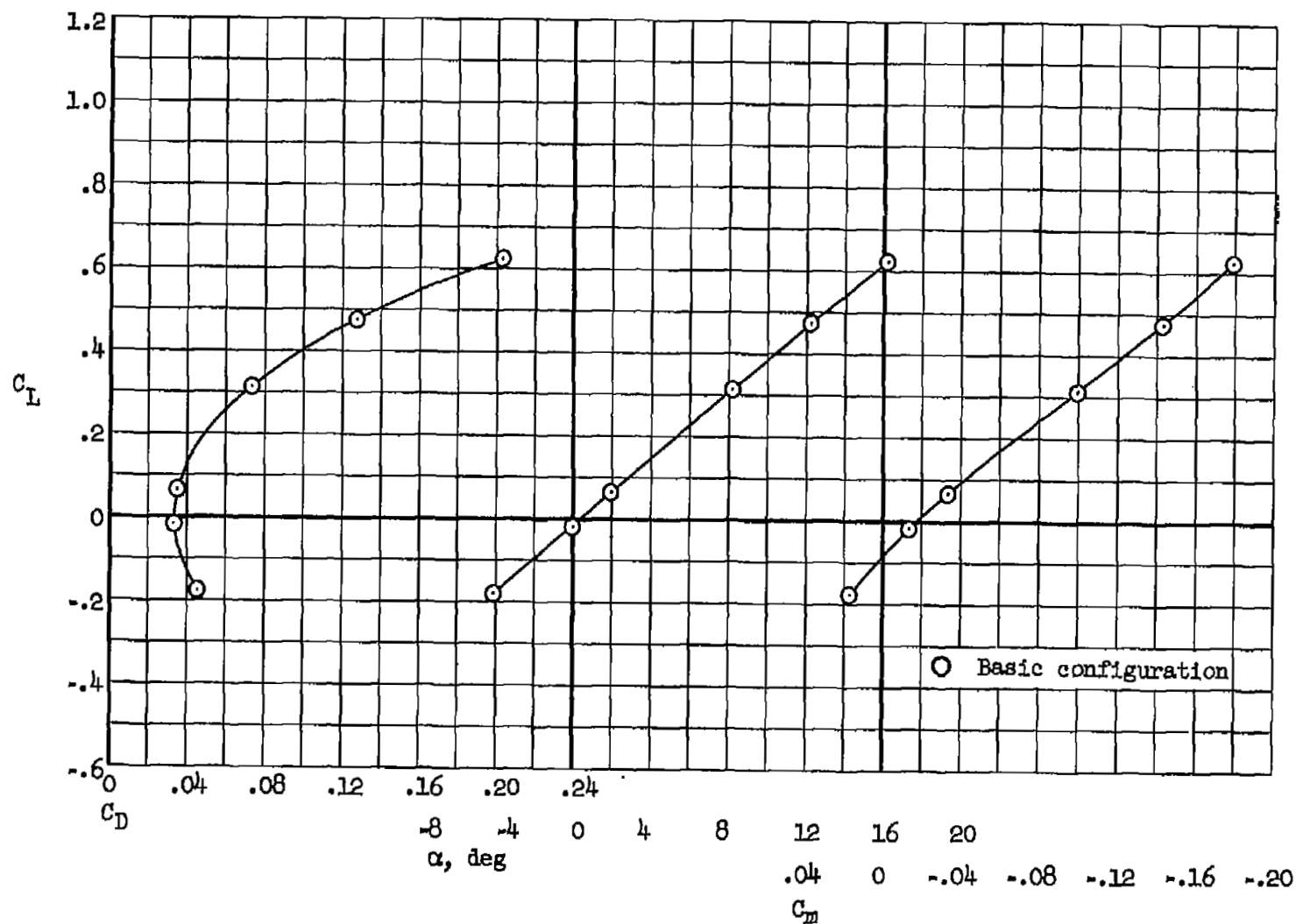
(e) $M = 2.35$

Figure 4.- Concluded.

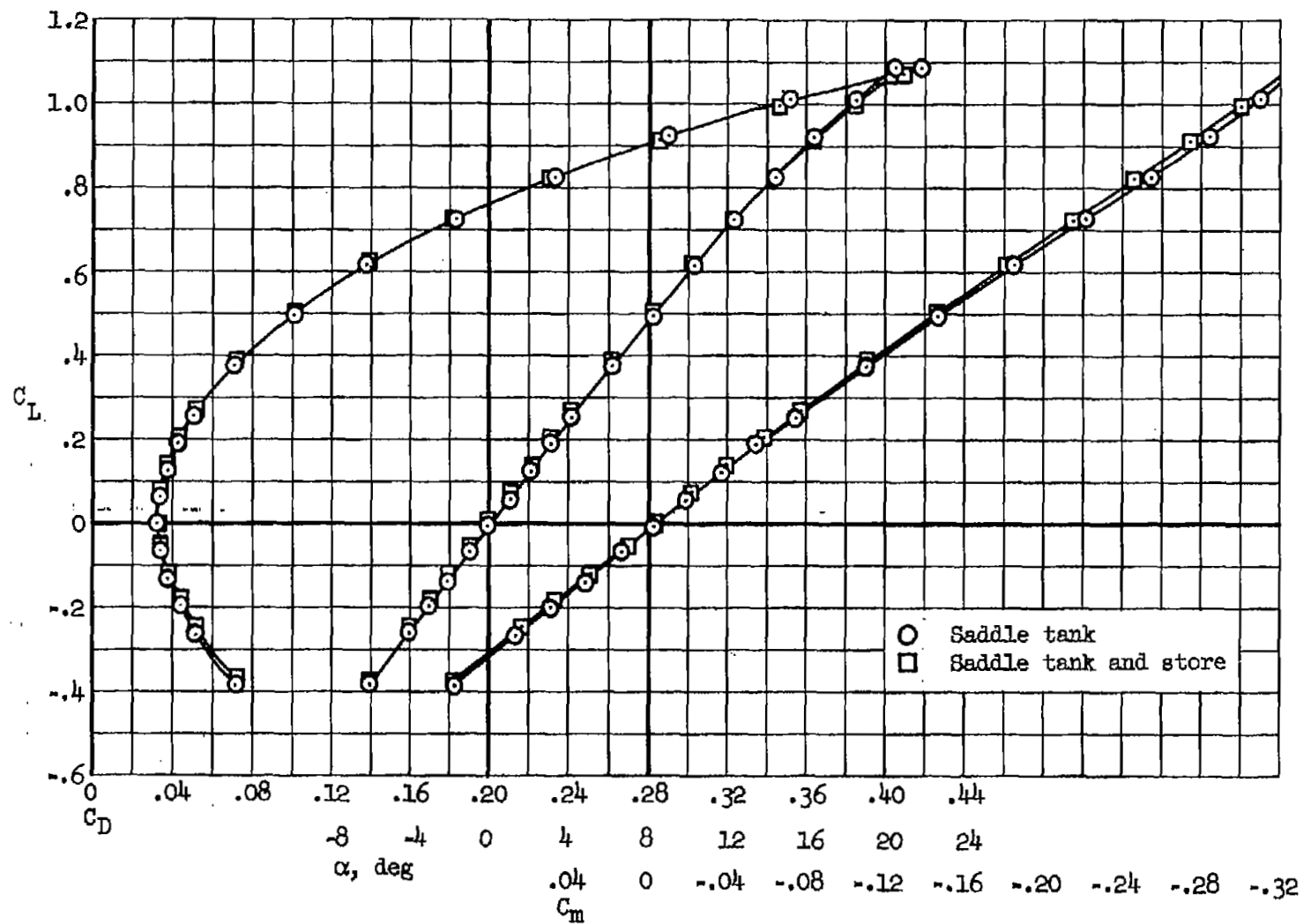
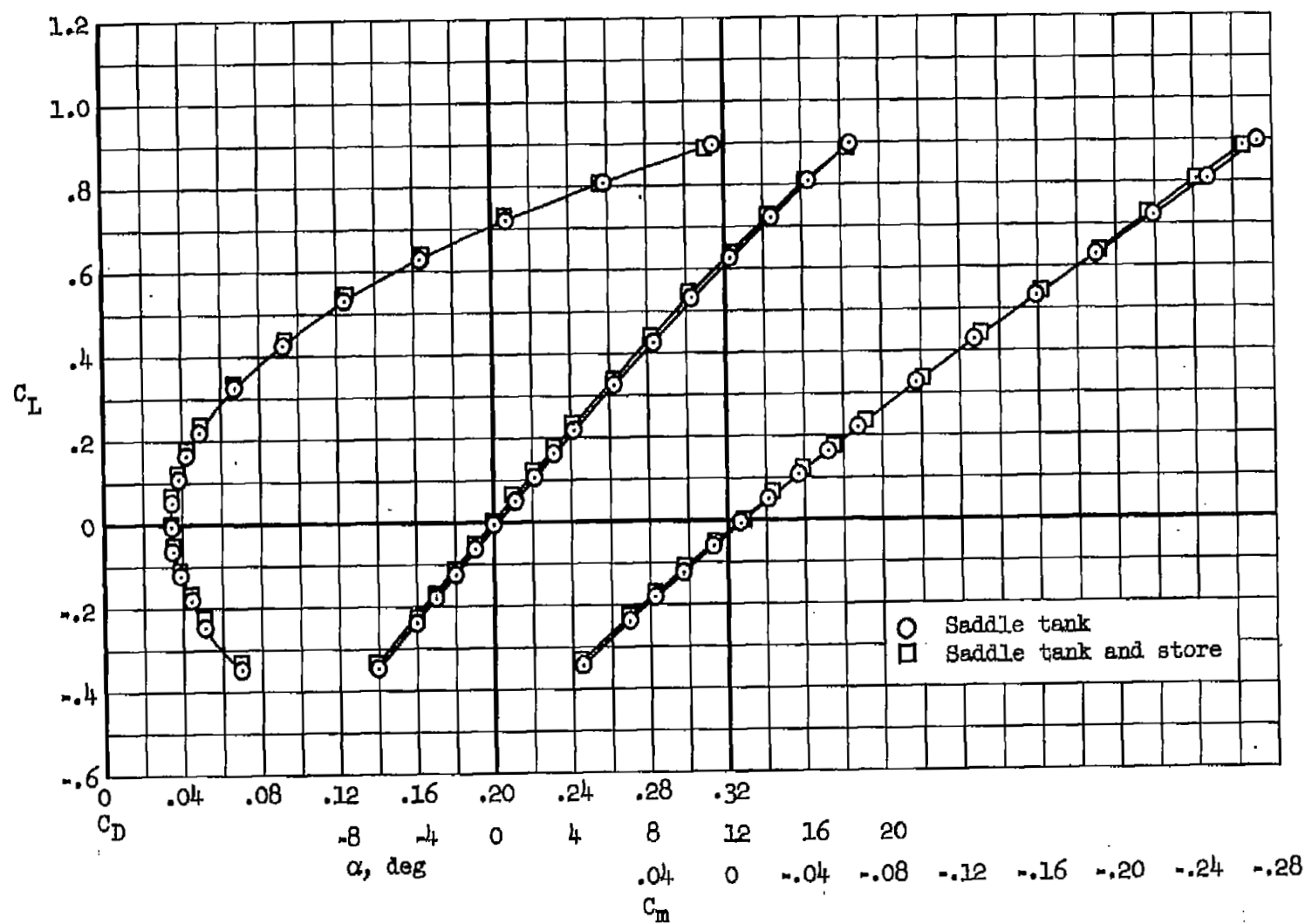
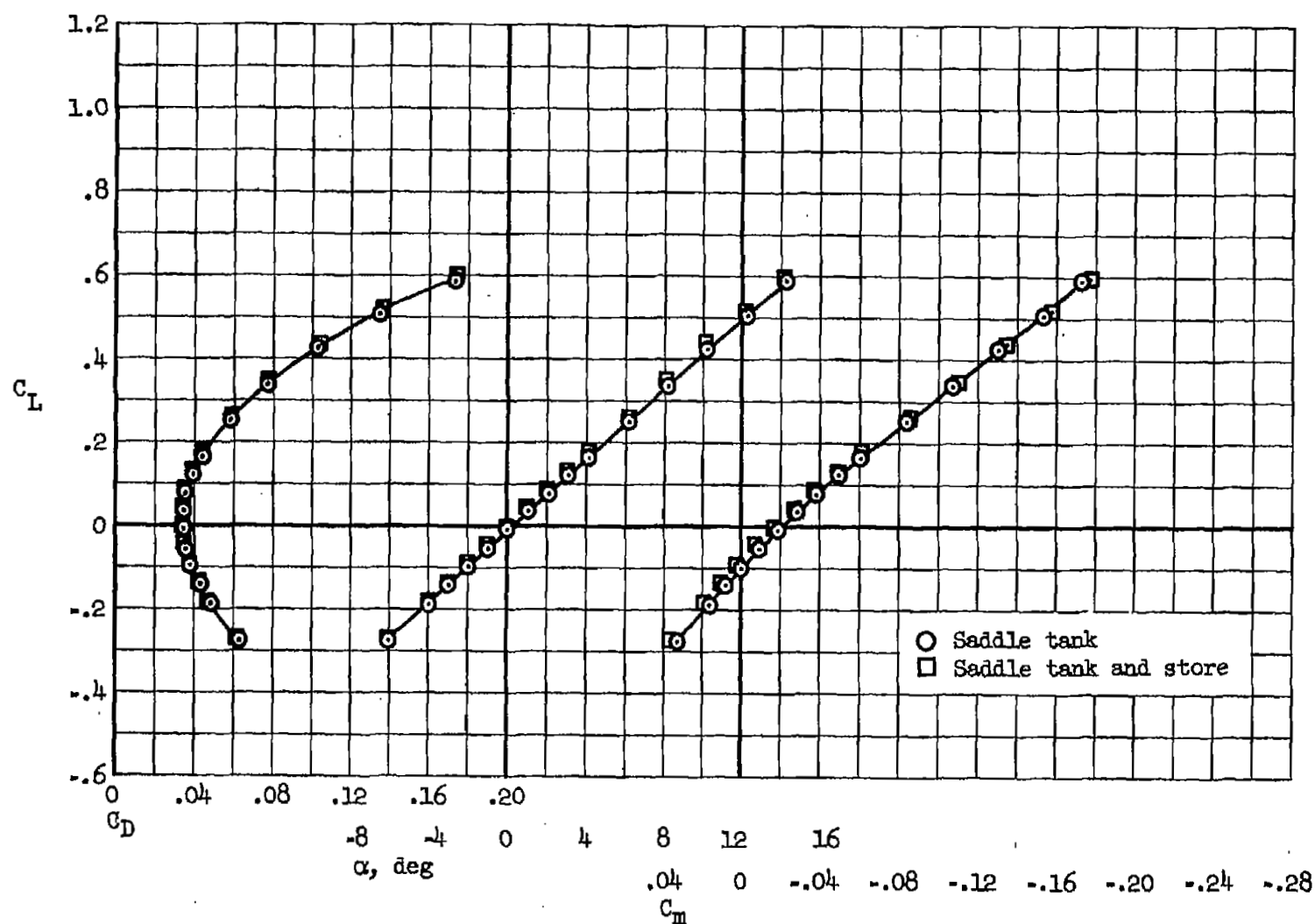
(a) $M = 1.6$

Figure 5.- Effects of store configurations on longitudinal characteristics.



(b) $M = 1.8$

Figure 5.- Continued.



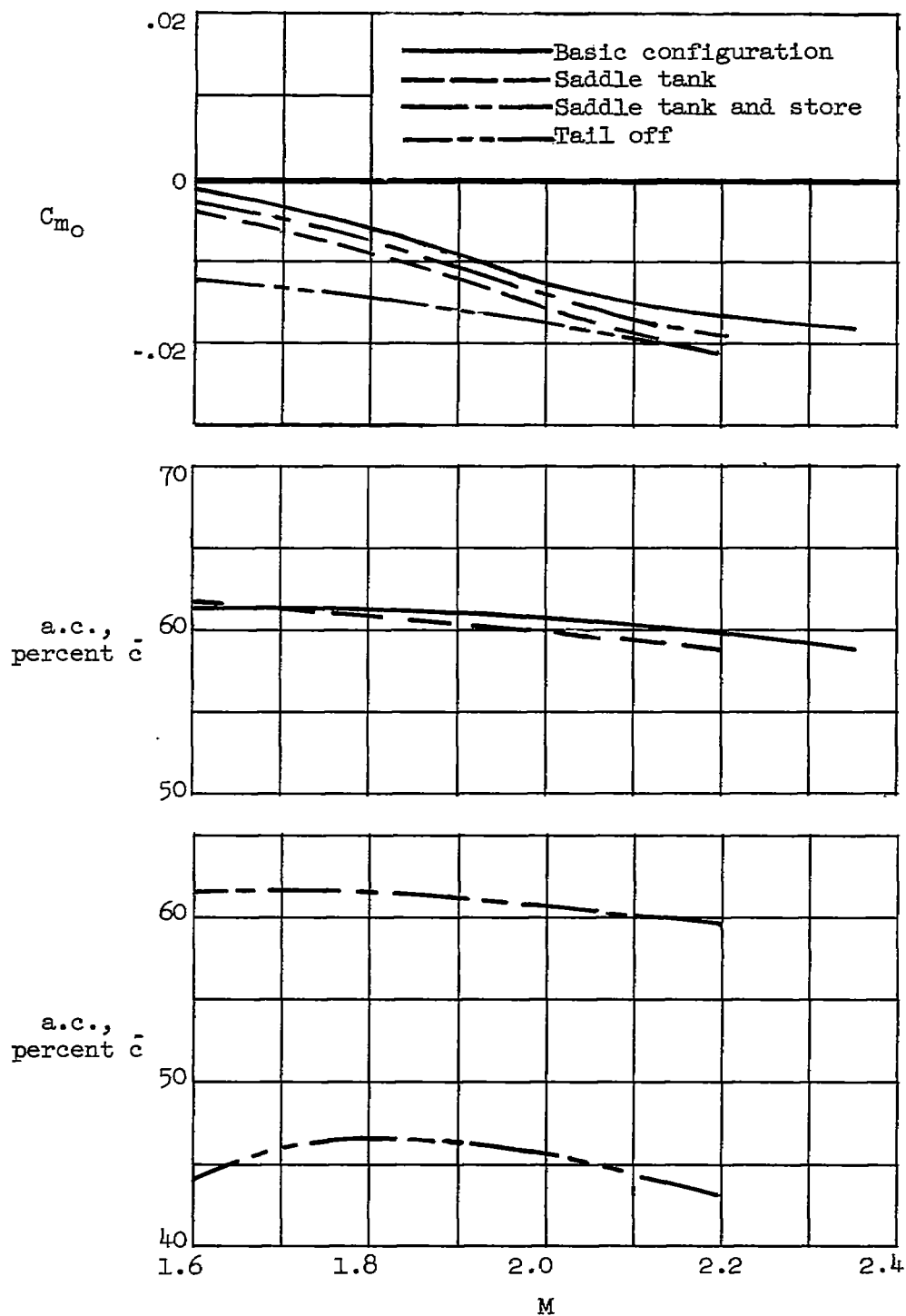


Figure 6.- Variation of pitching moment at zero lift and aerodynamic center with Mach number for configurations tested.

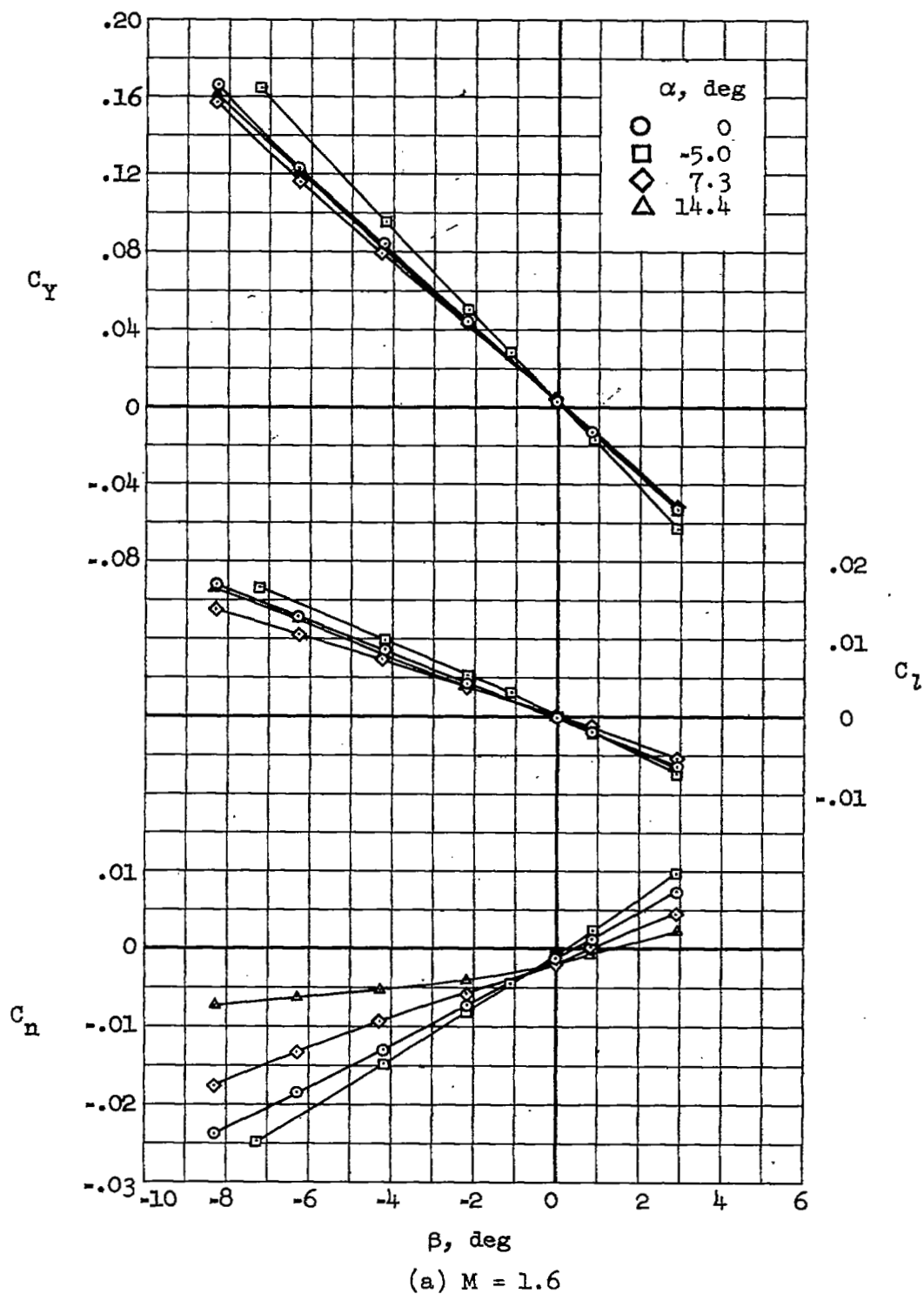


Figure 7.- Angle-of-attack effects on lateral characteristics of the basic configuration.

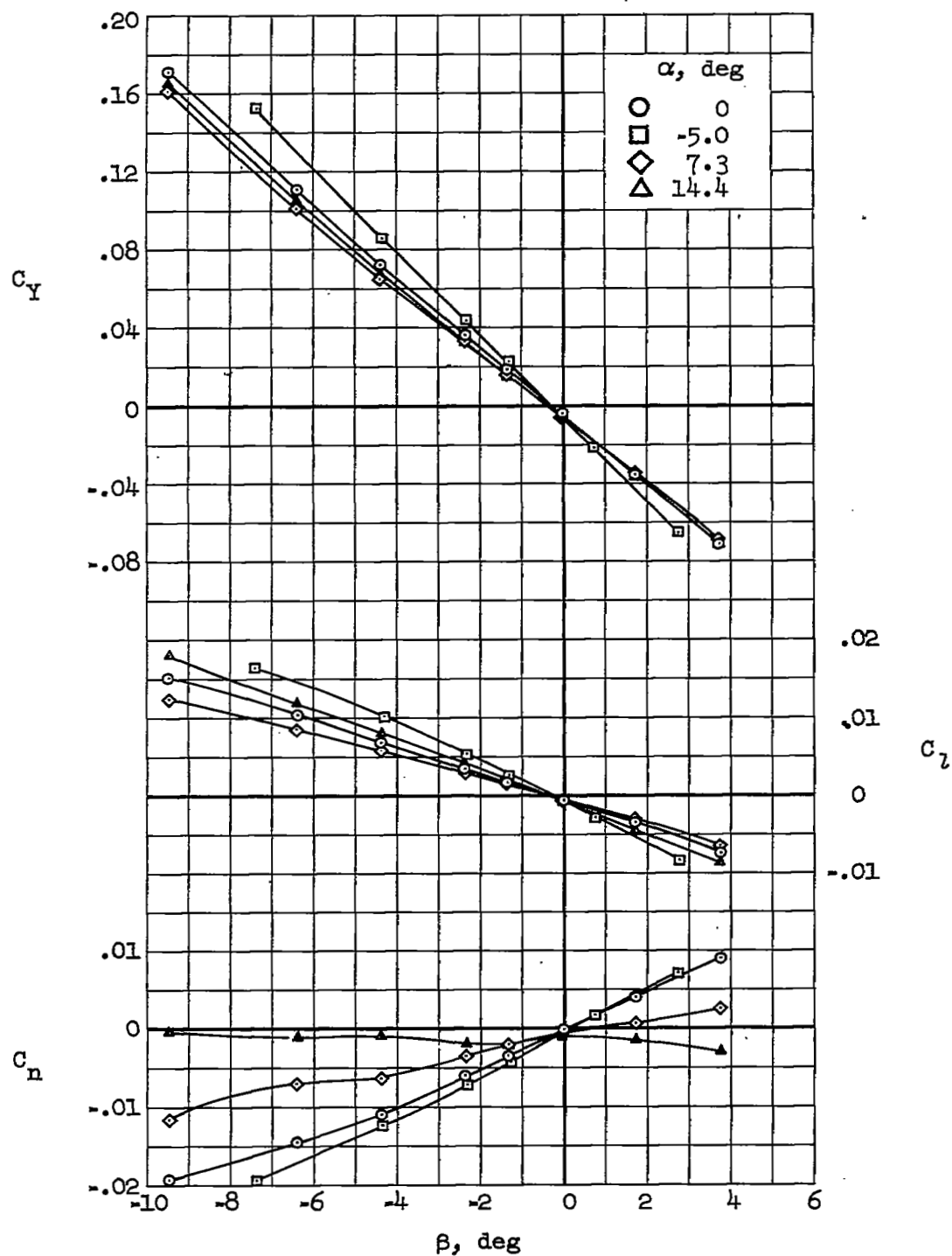
(b) $M = 1.8$

Figure 7.- Continued.

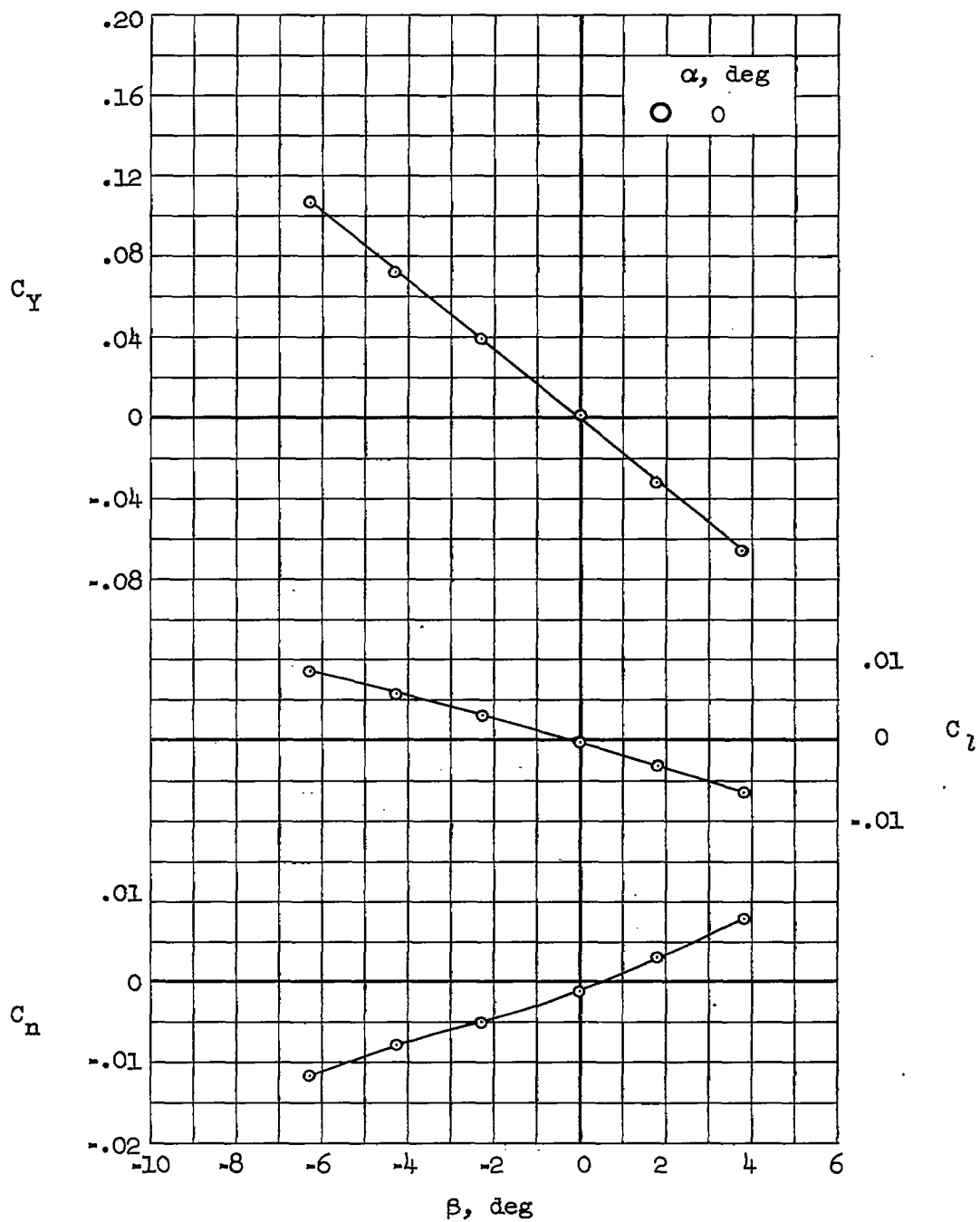
(c) $M = 2.0$

Figure 7.- Continued.

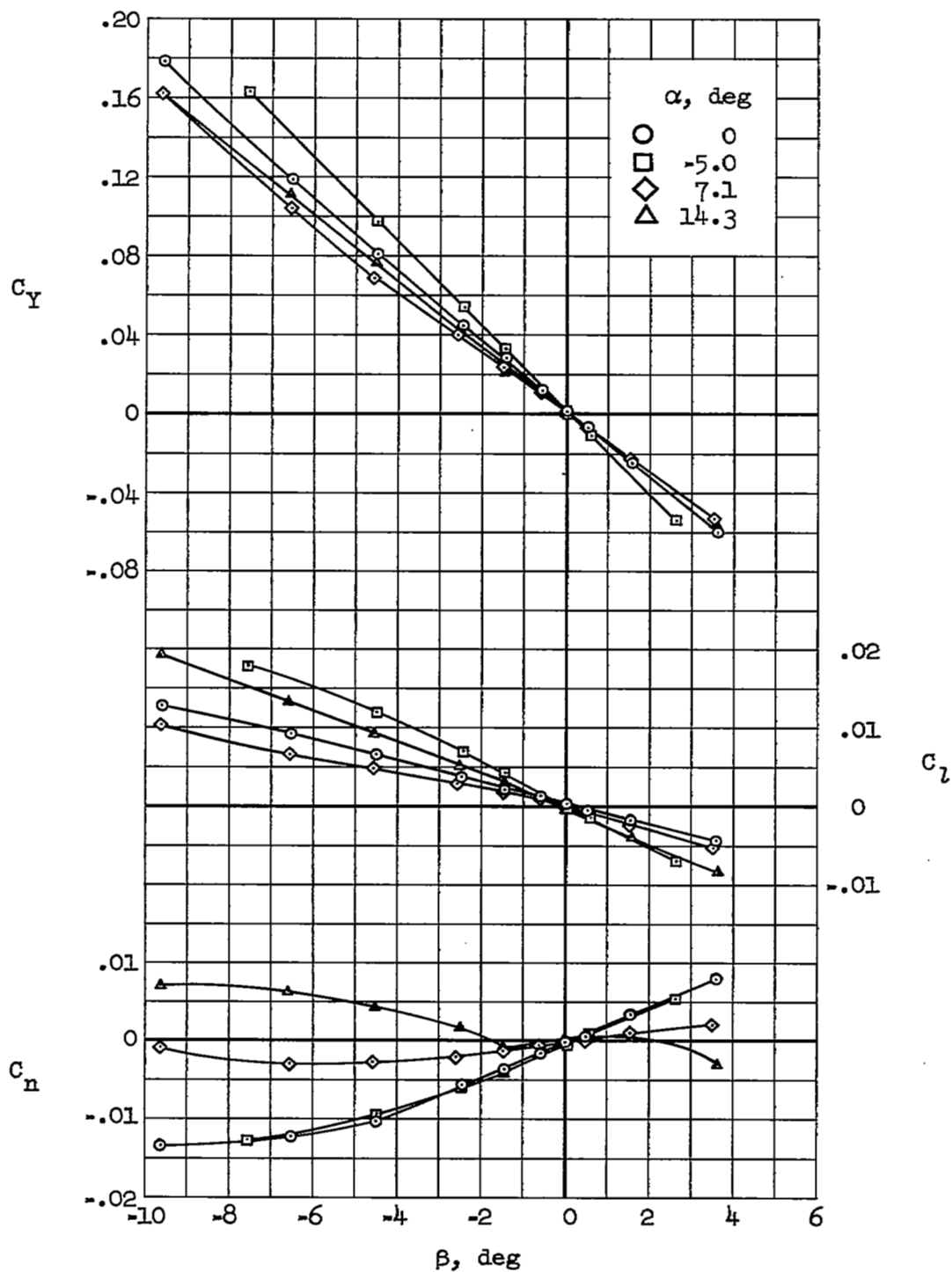


Figure 7.- Continued.

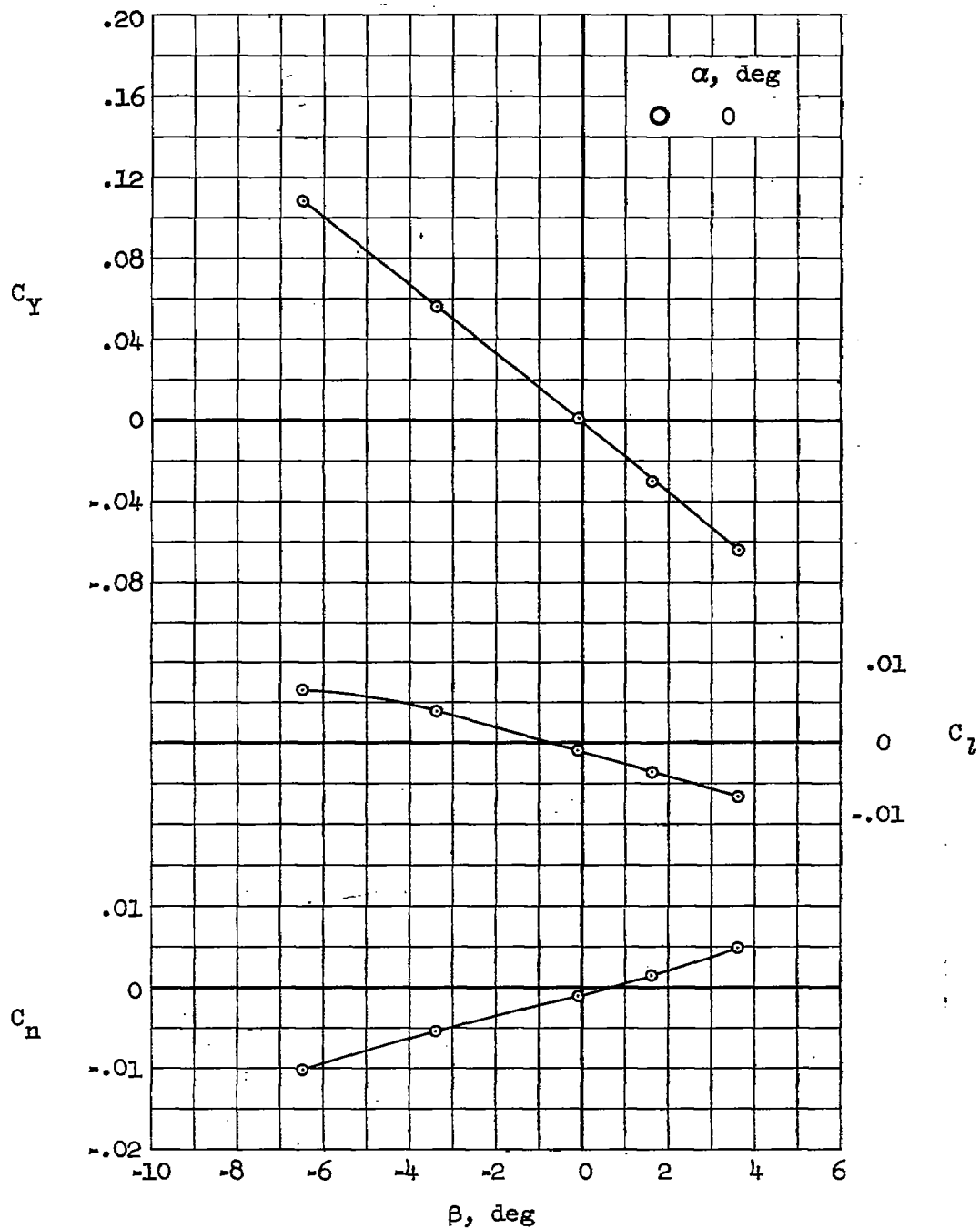
(e) $M = 2.35$

Figure 7.- Concluded.

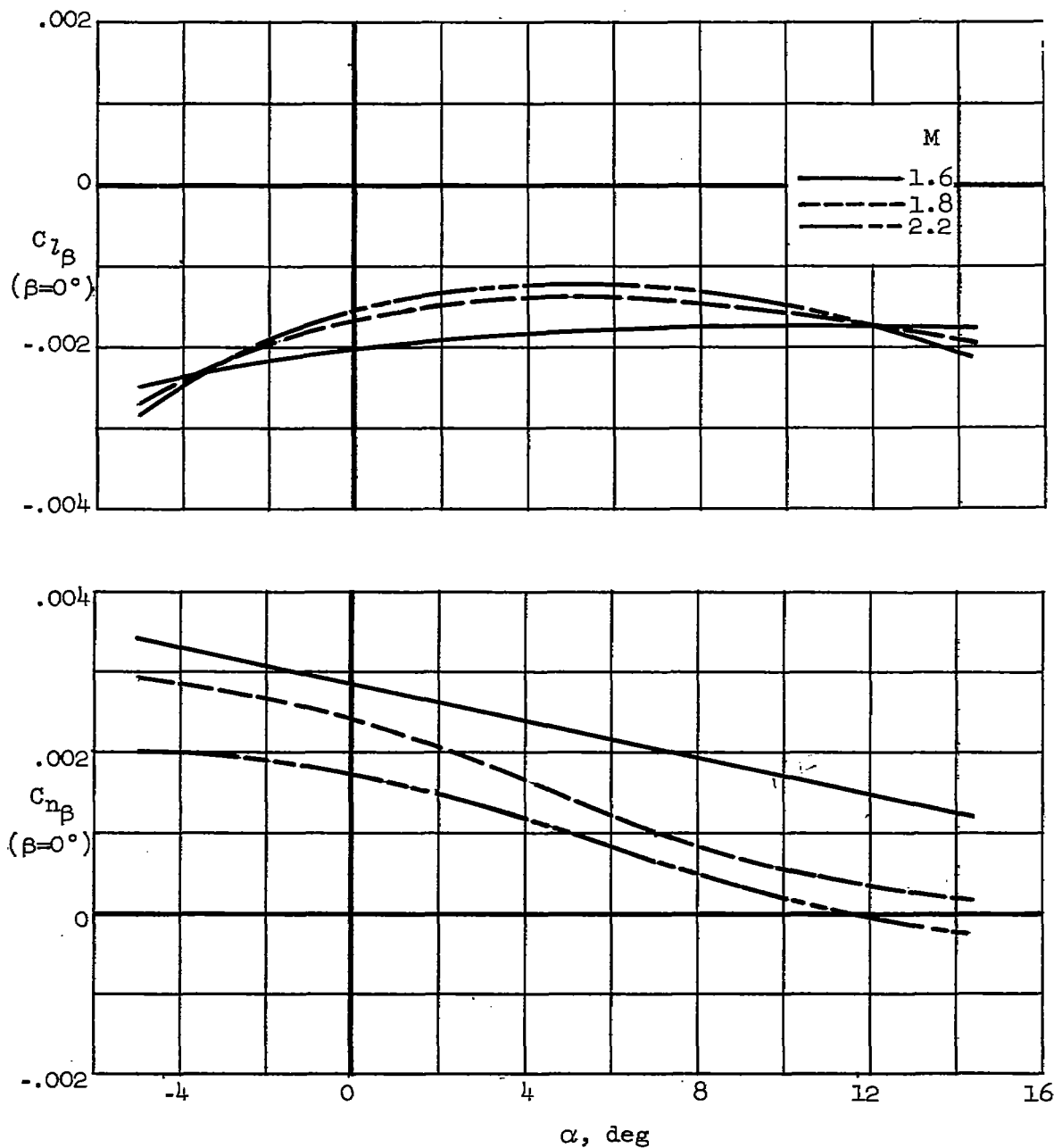


Figure 8.- Variation of rolling-moment and yawing-moment derivatives with angle of attack for the basic configuration.

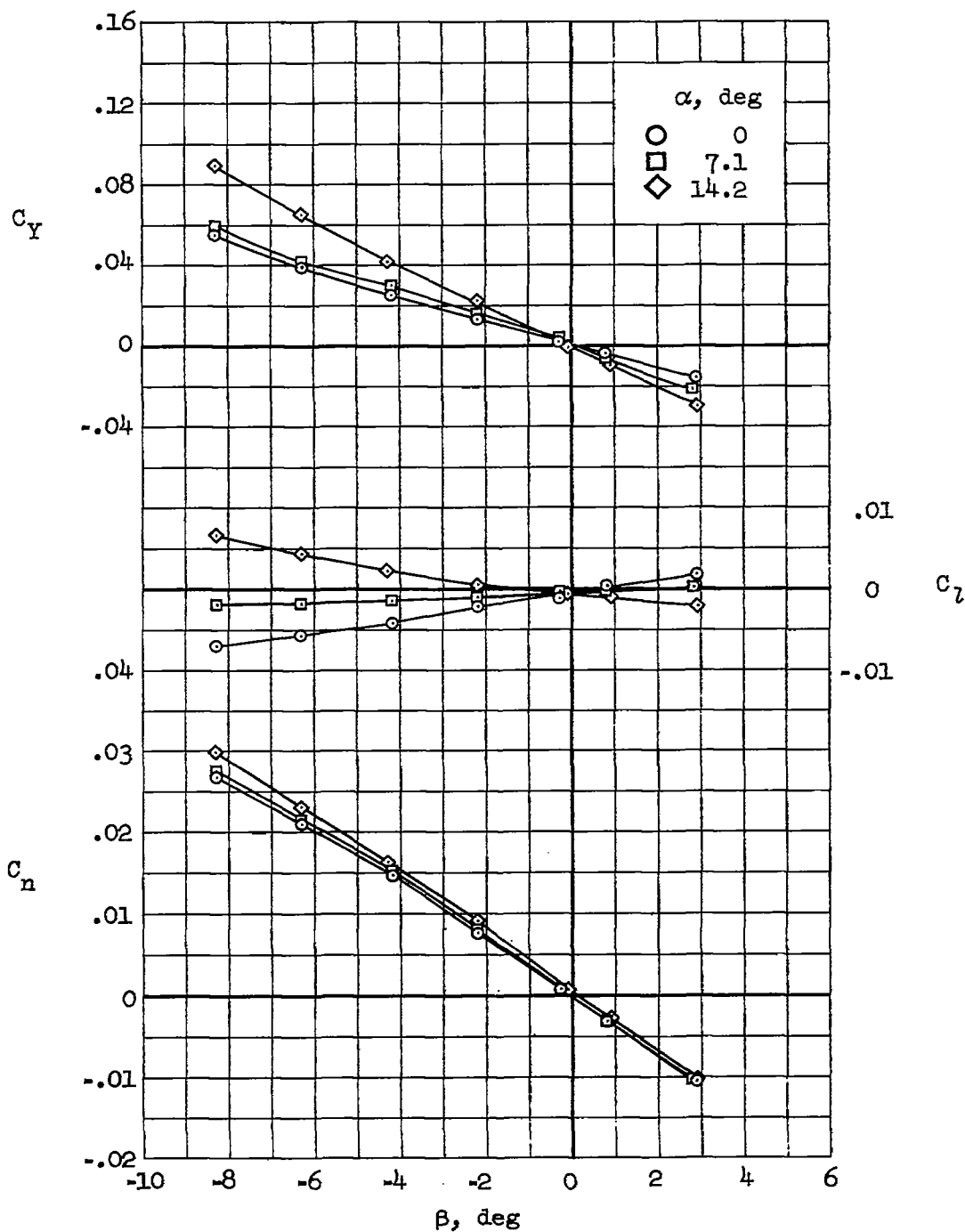
(a) $M = 1.6$

Figure 9.- Angle-of-attack effects on lateral characteristics of the vertical tail off configuration.

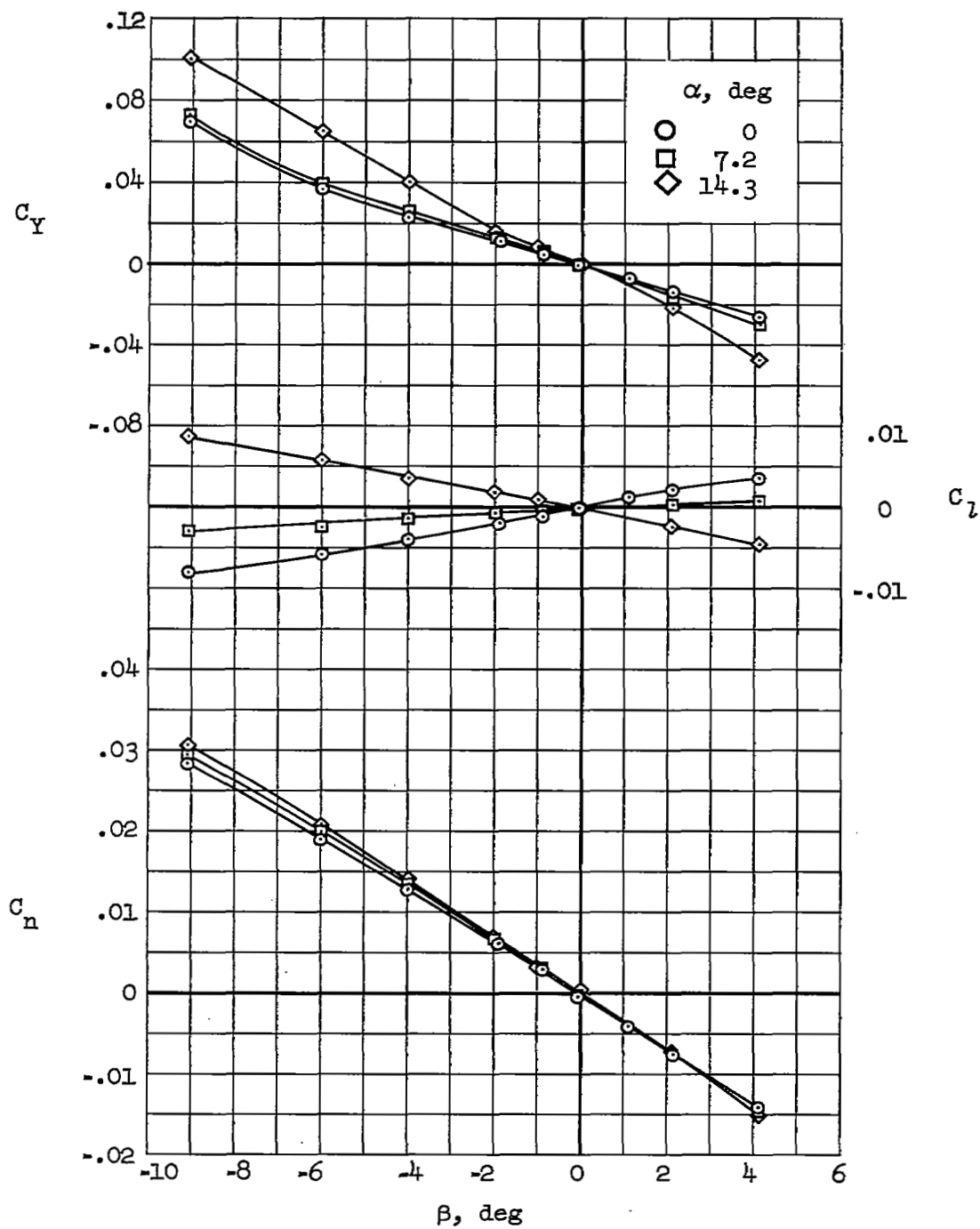
(b) $M = 1.8$

Figure 9.- Continued.

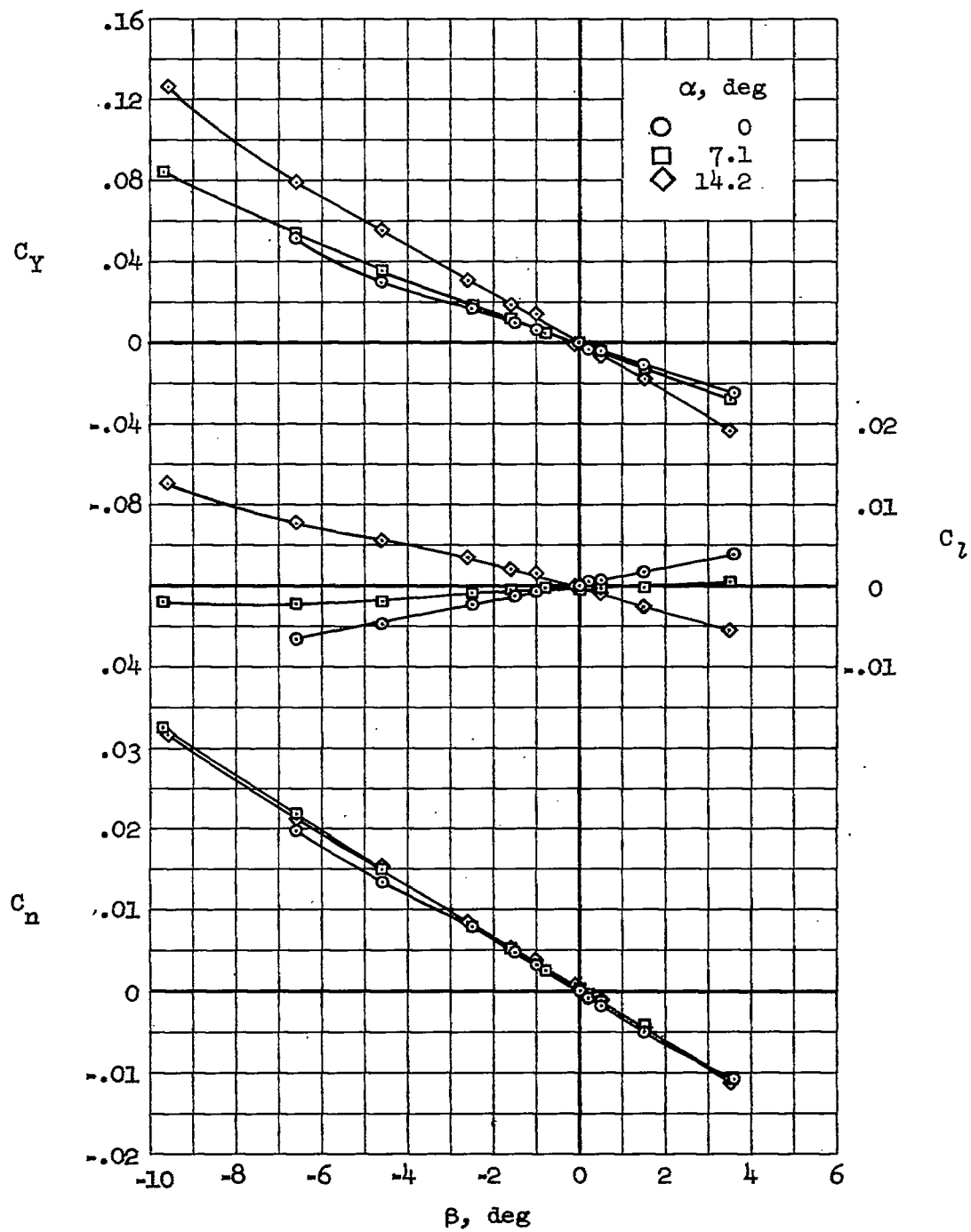
(c) $M = 2.2$

Figure 9.- Concluded.

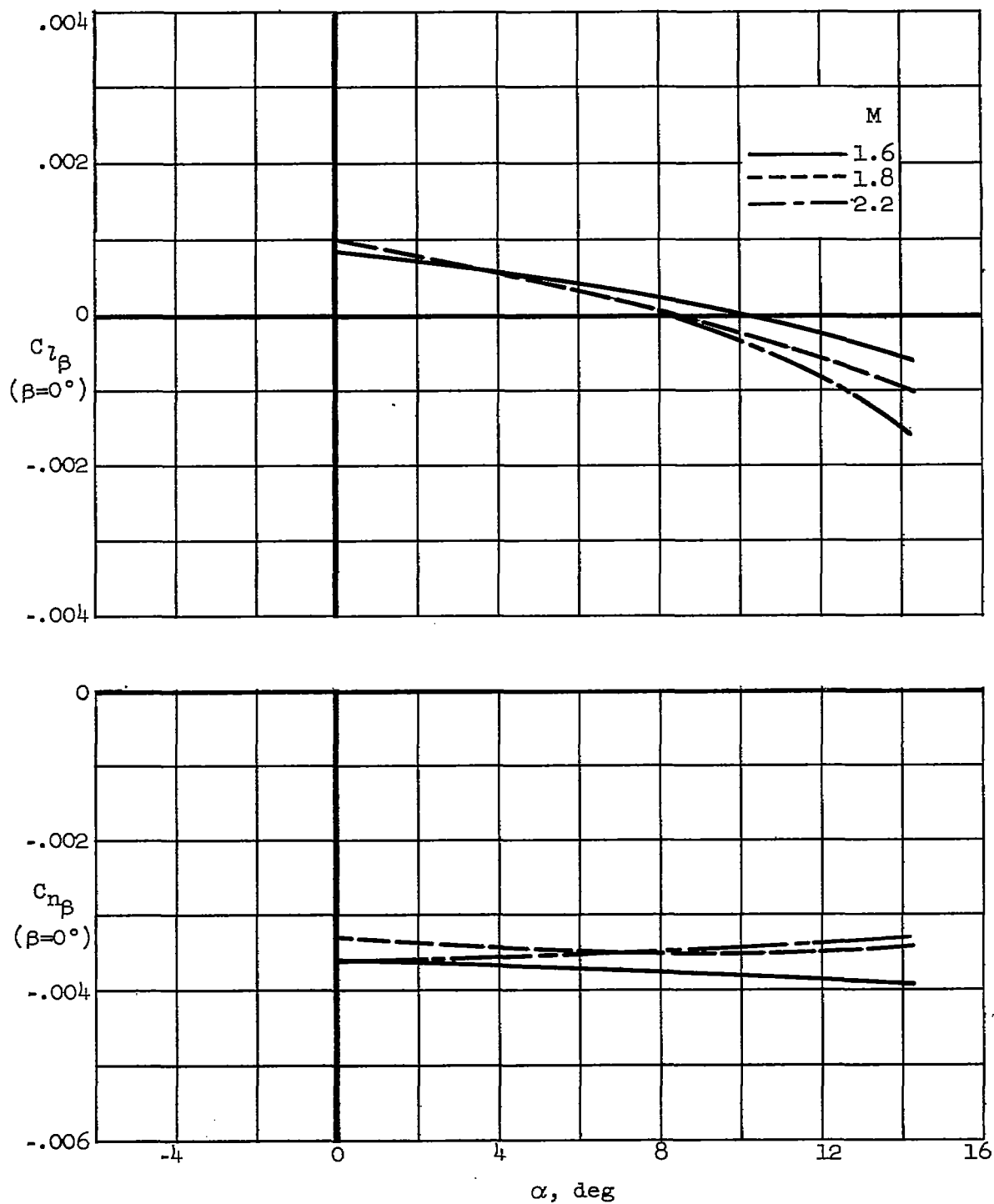
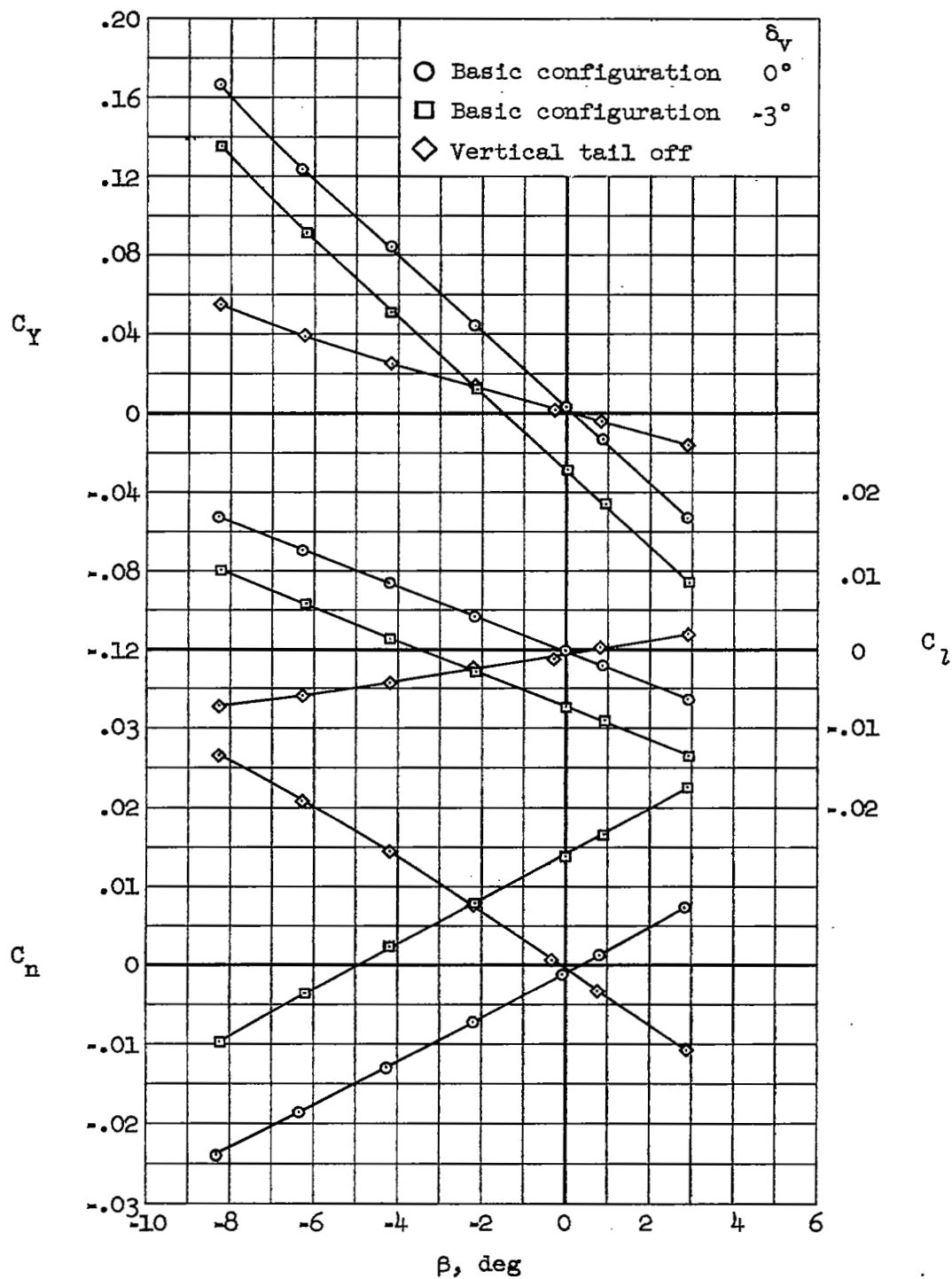


Figure 10.- Variation of rolling-moment and yawing-moment derivatives with angle of attack for the vertical tail off configuration.

(a) $M = 1.6$ Figure 11.- Effect of vertical tail on lateral characteristics of basic configuration; $\alpha = 0^\circ$.

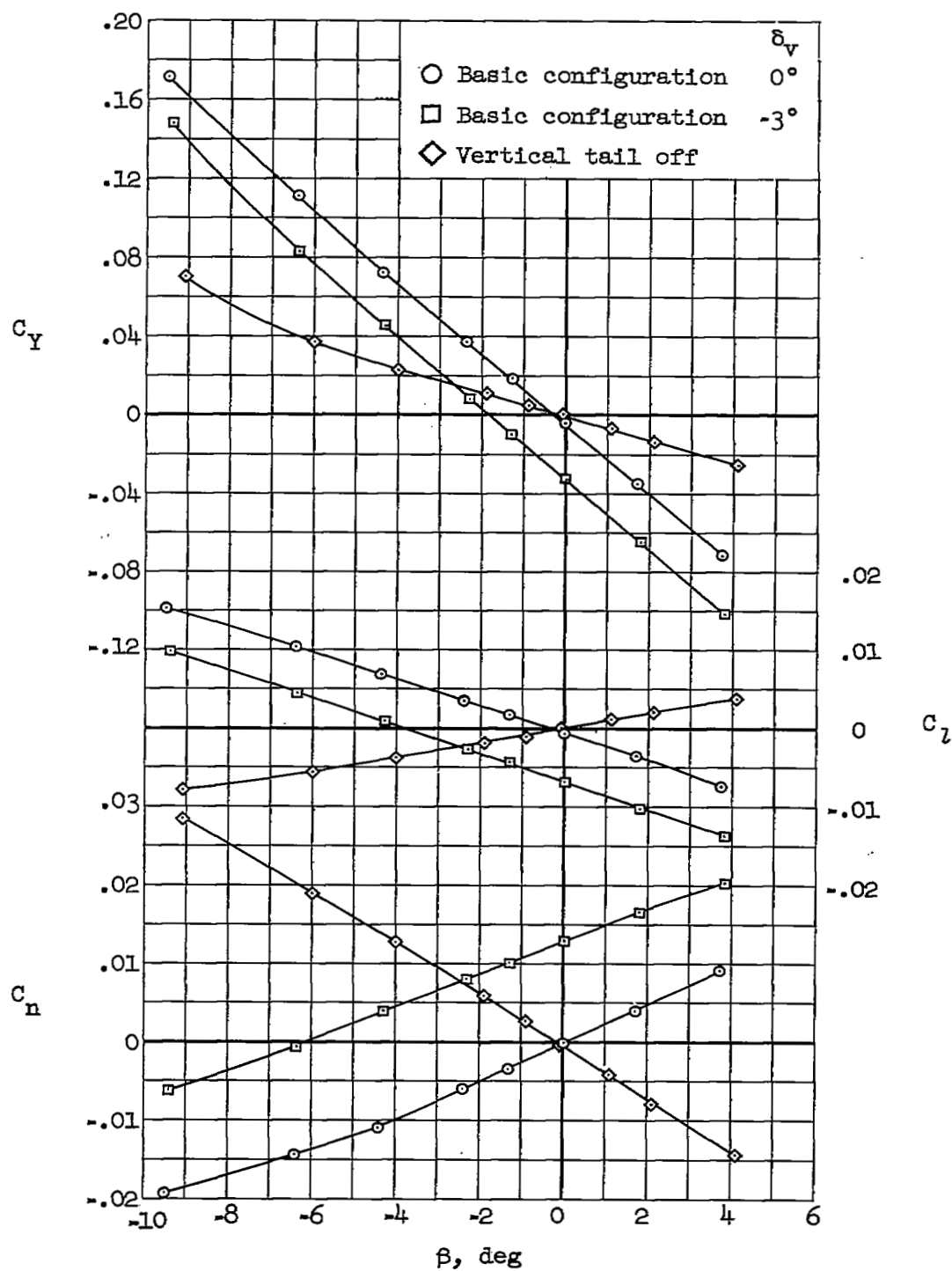
(b) $M = 1.8$

Figure 11.- Continued.

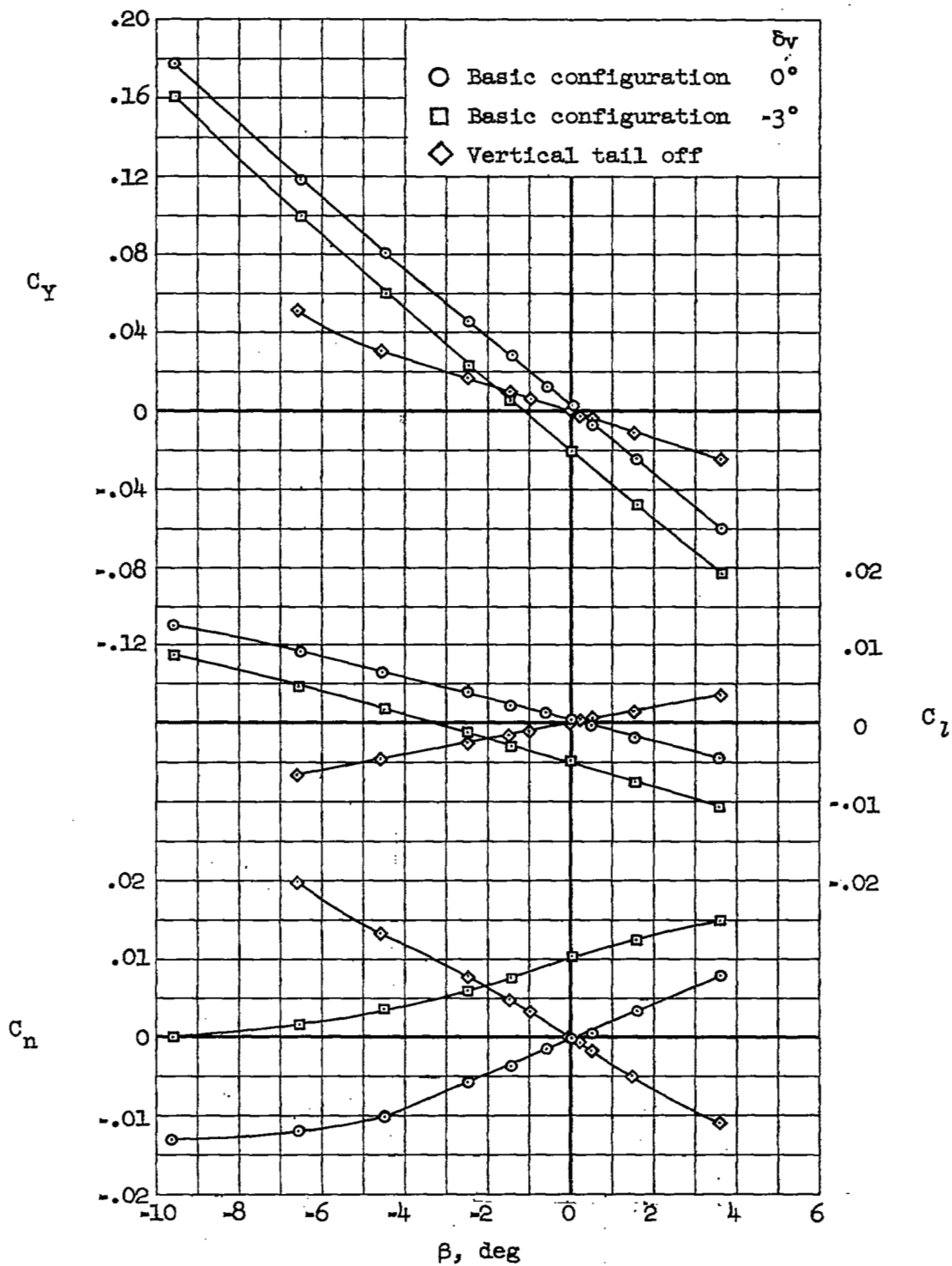
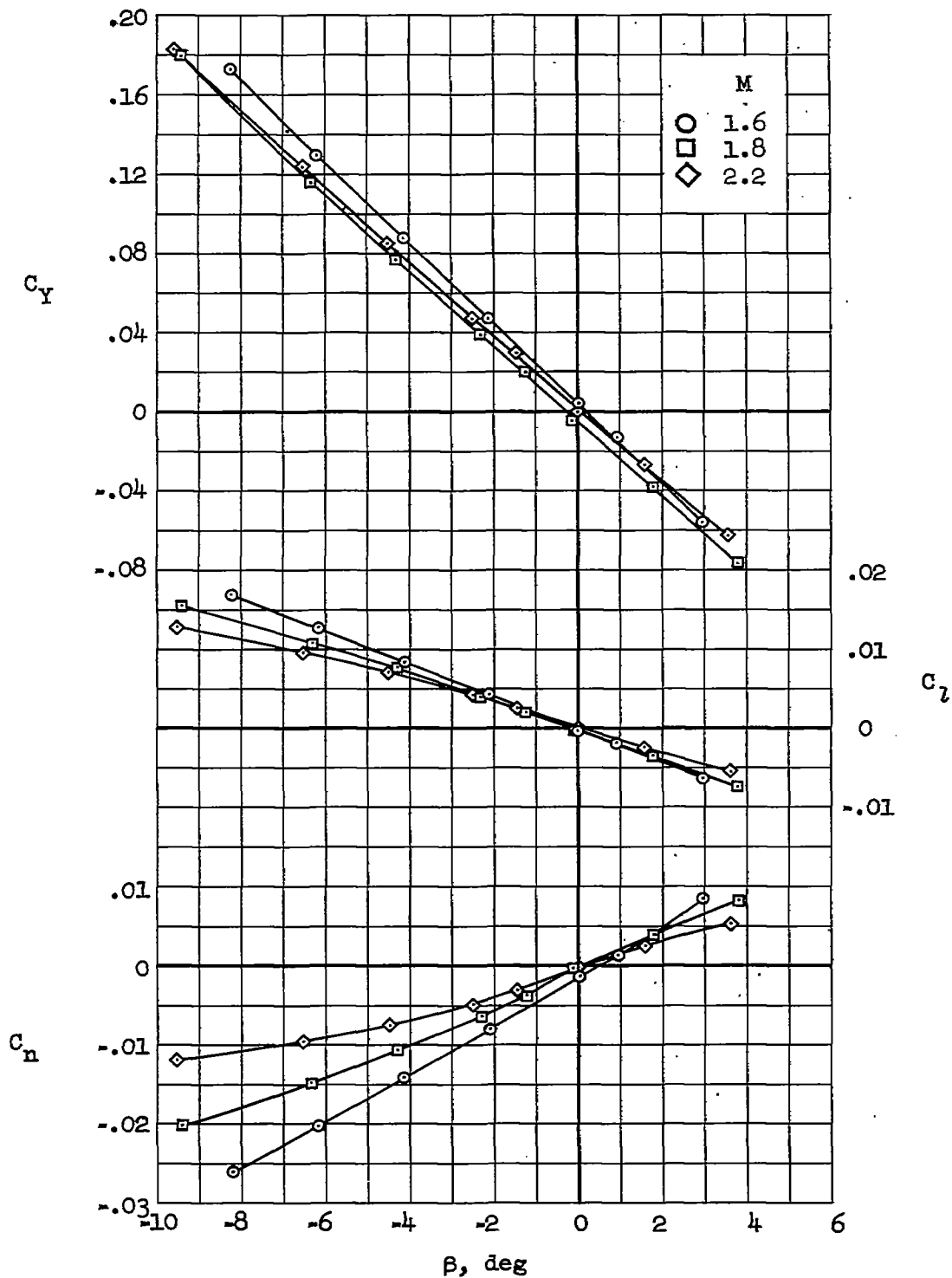
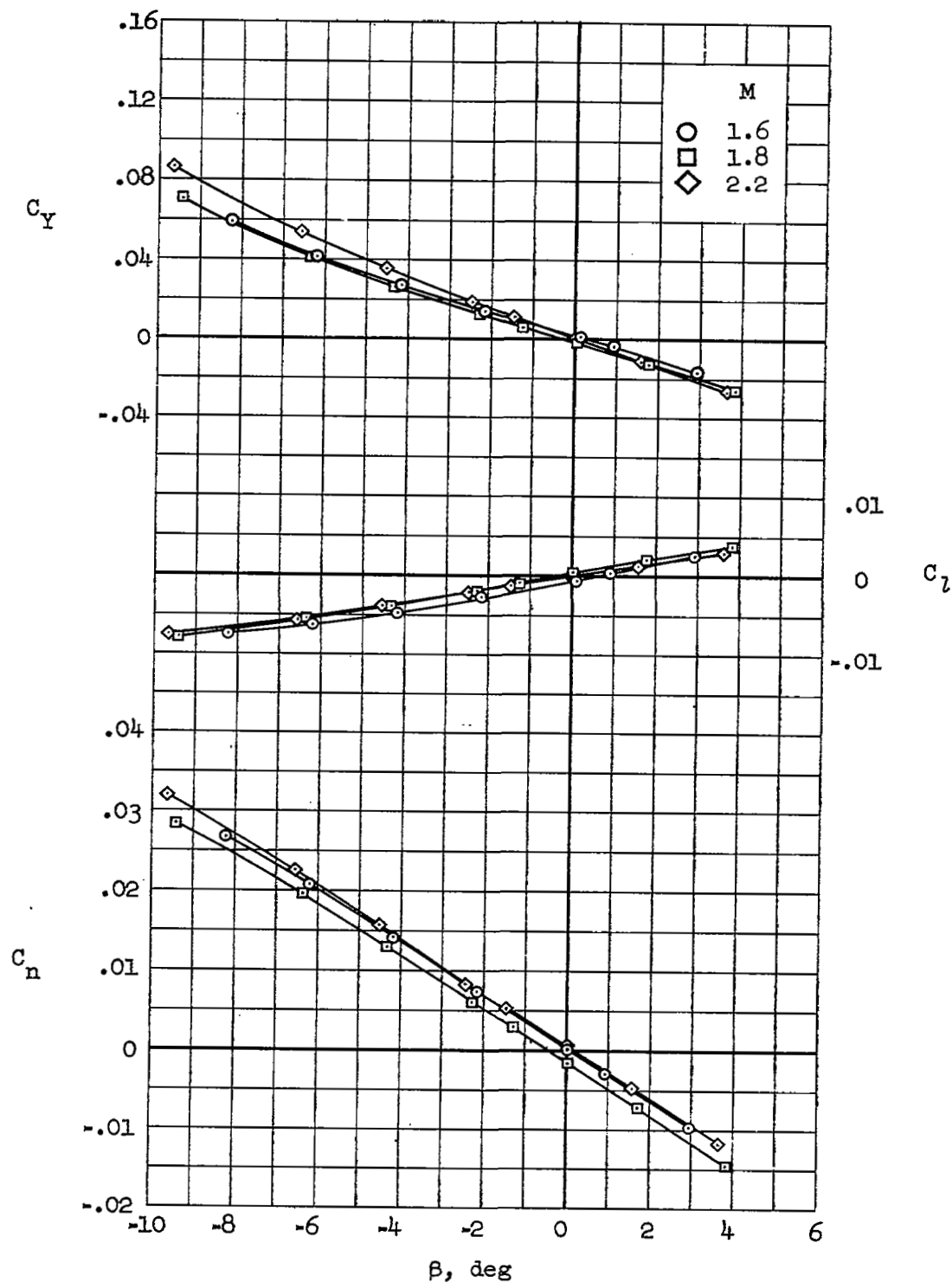
(c) $M = 2.2$

Figure 11.- Concluded.



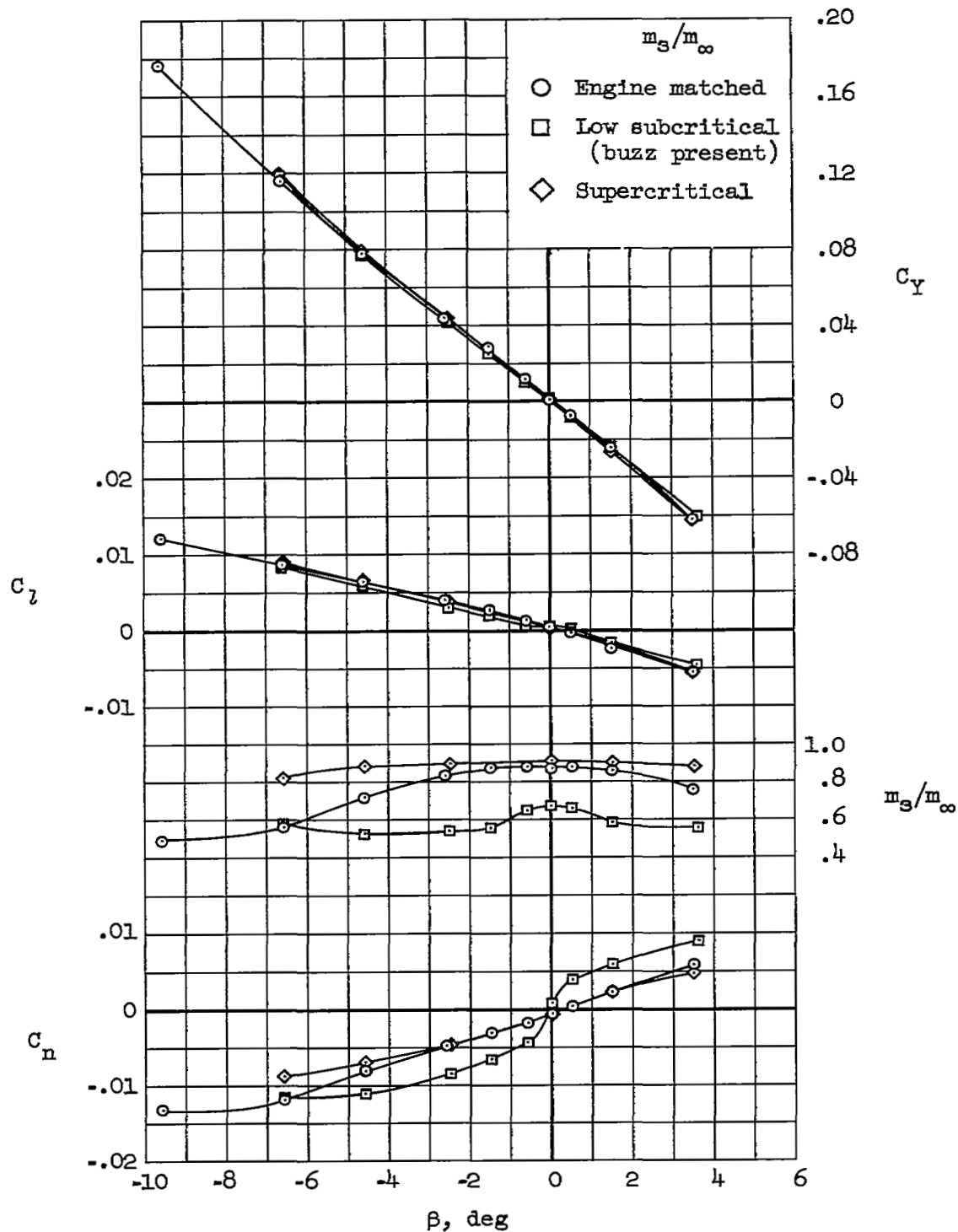
(a) Vertical tail on.

Figure 12.- Effect of vertical tail on lateral characteristics of the saddle tank and store configuration; $\alpha = 0^\circ$.



(b) Vertical tail off.

Figure 12.- Concluded.



(a) $\alpha = 0^\circ$.

Figure 13.- Effect of mass-flow ratio on lateral characteristics of basic configuration; $M = 2.2$.

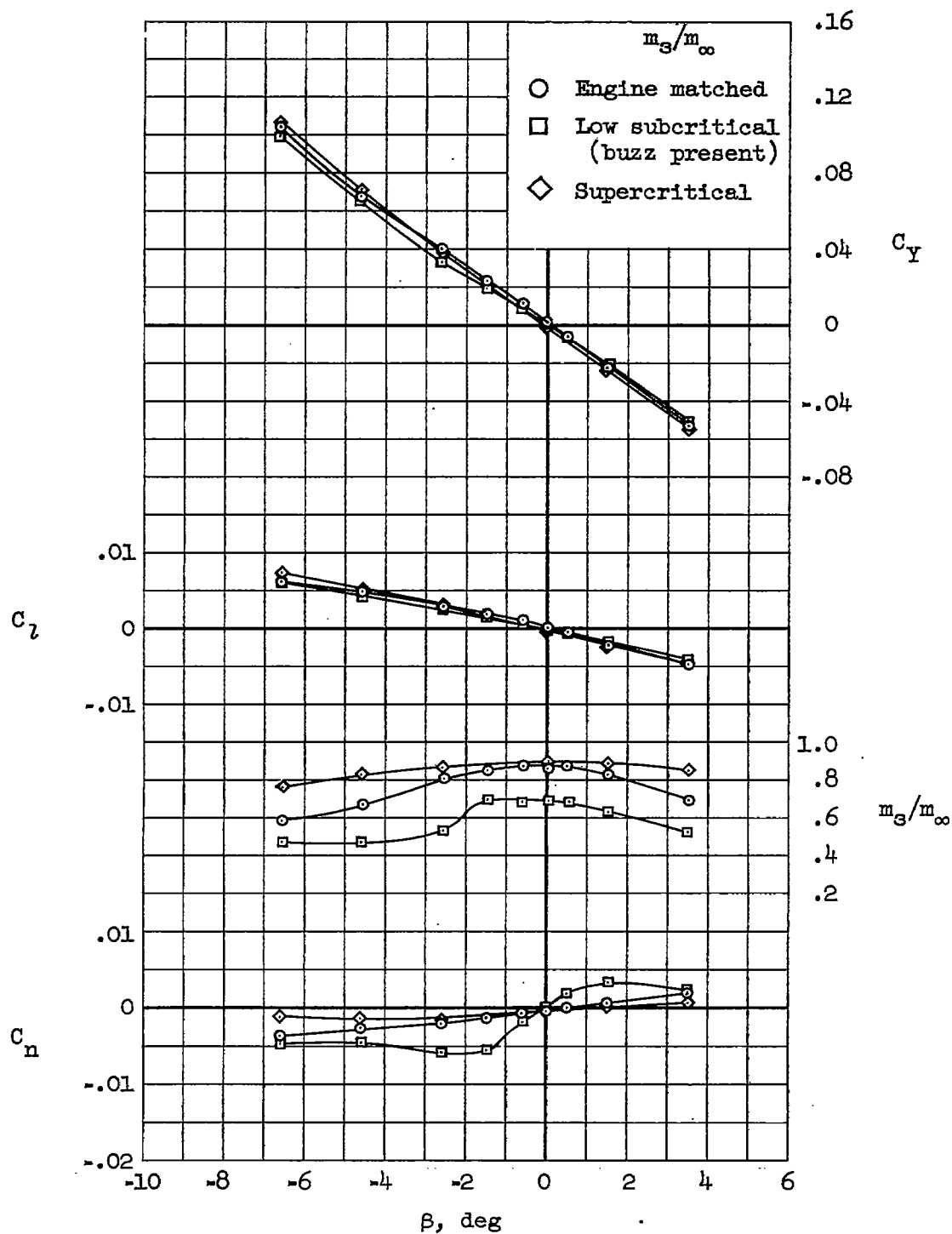
(b) $\alpha = 7^\circ$

Figure 13.- Continued.

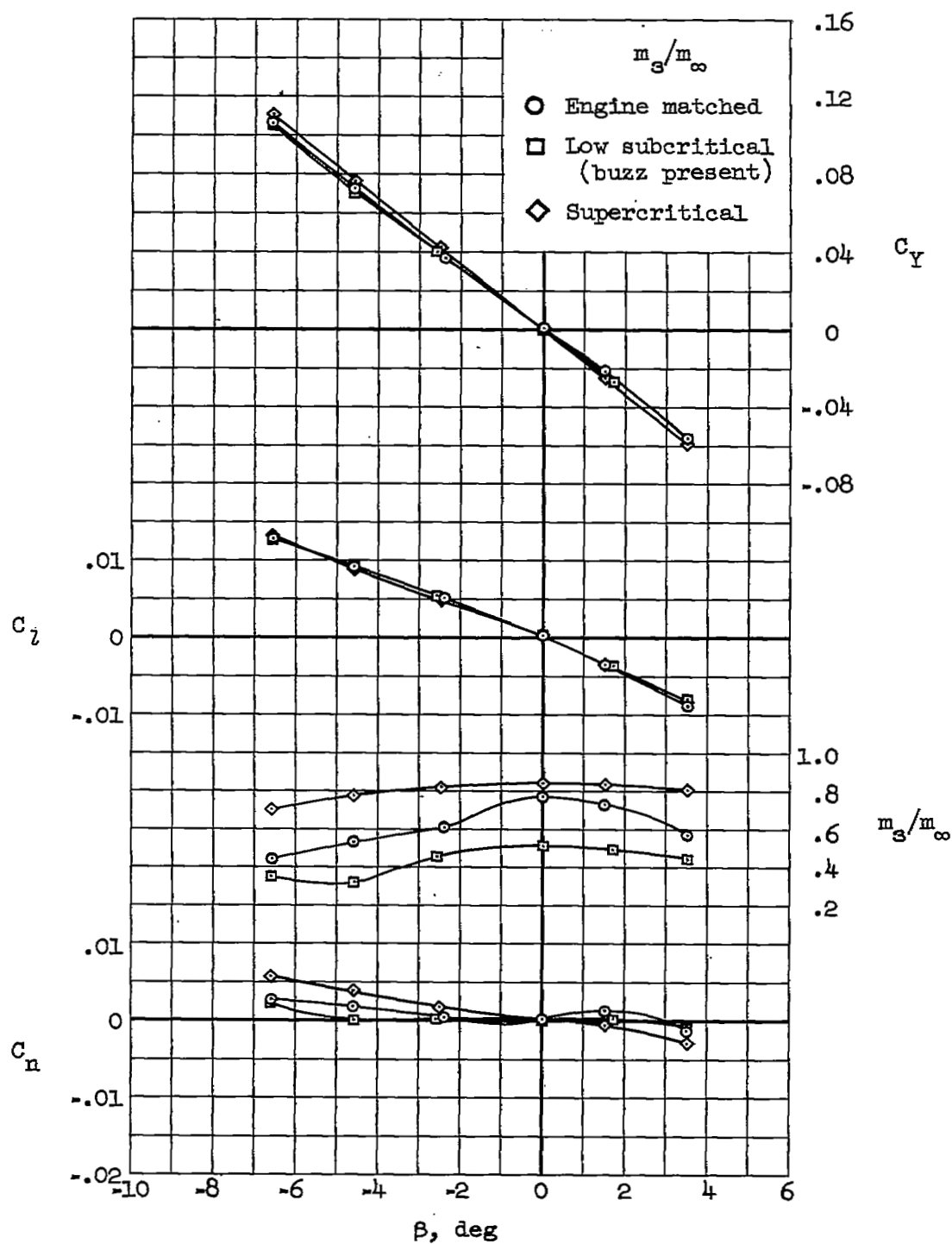
(c) $\alpha = 14^\circ$

Figure 13.- Concluded.

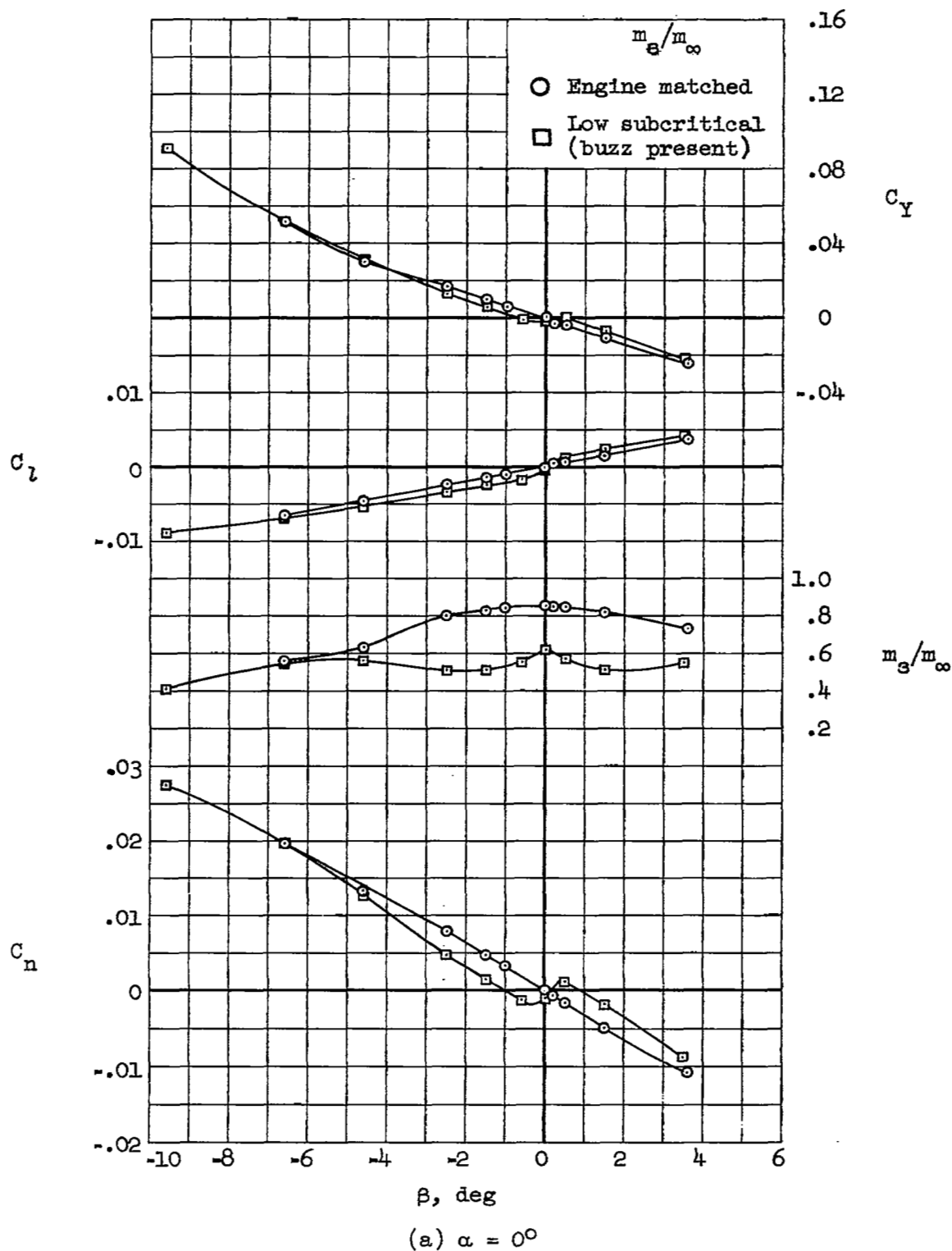


Figure 14.- Effect of mass-flow ratio on lateral characteristics of vertical tail off configuration; $M = 2.2$.

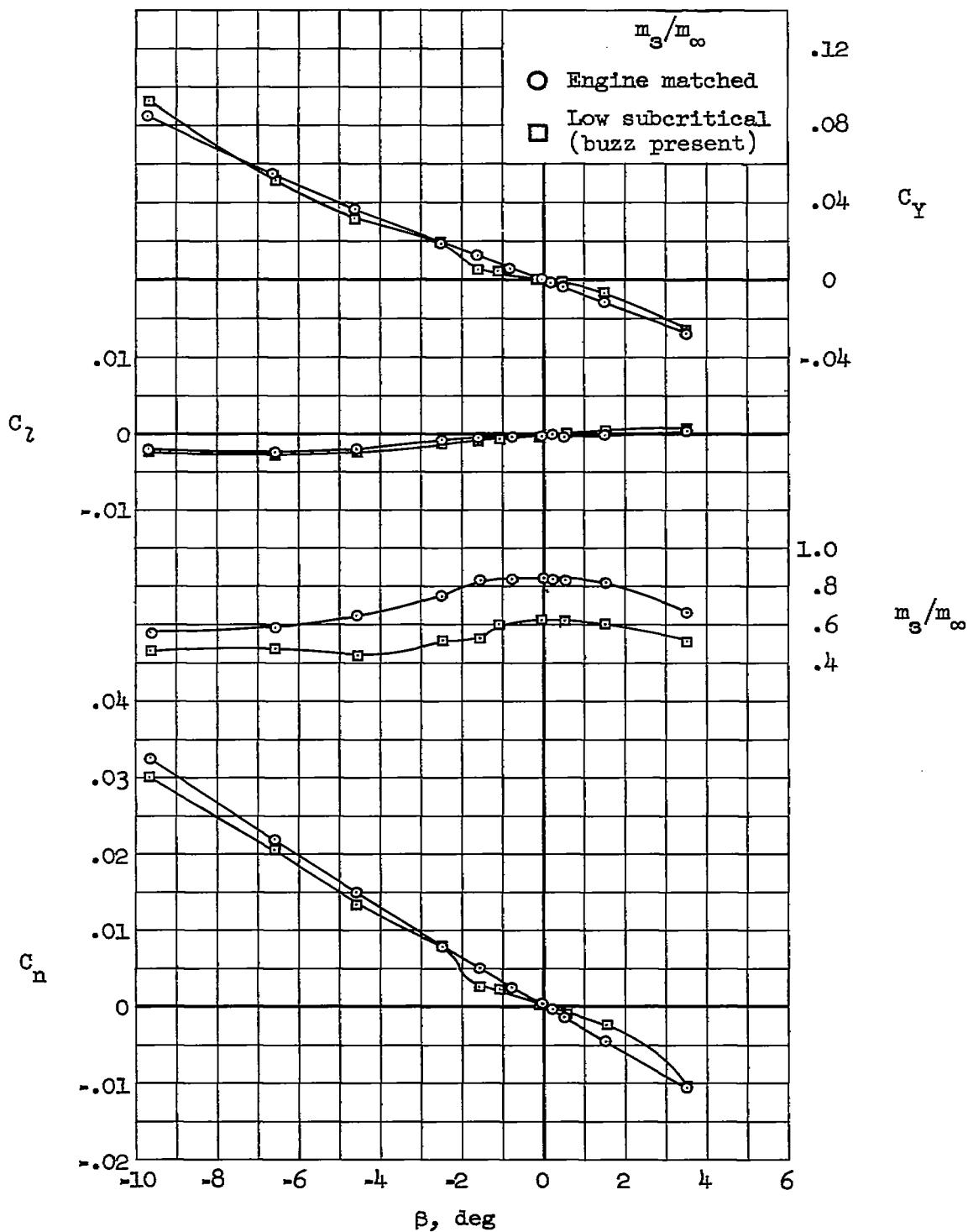
(b) $\alpha = 7^\circ$

Figure 14.- Continued.

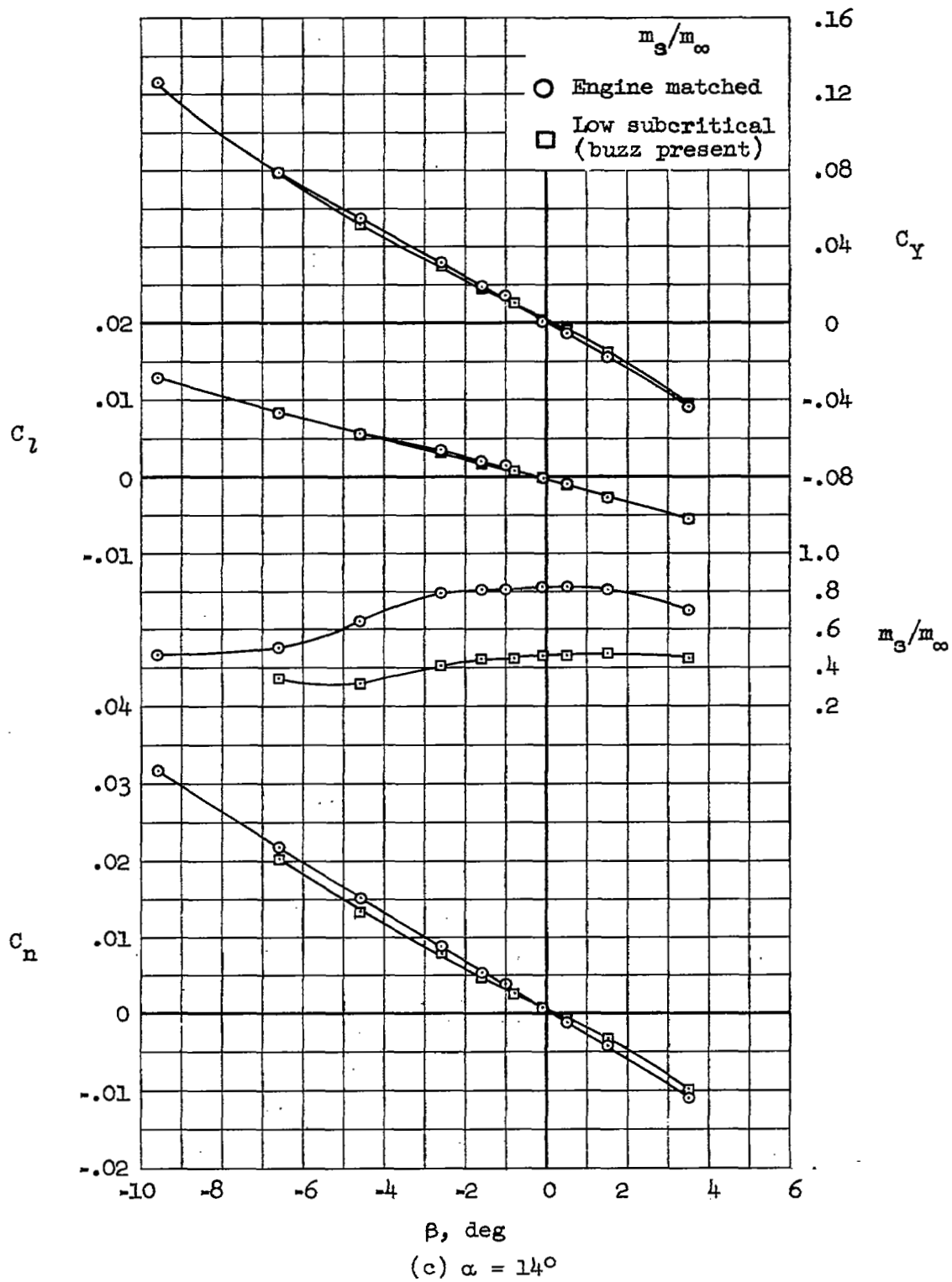
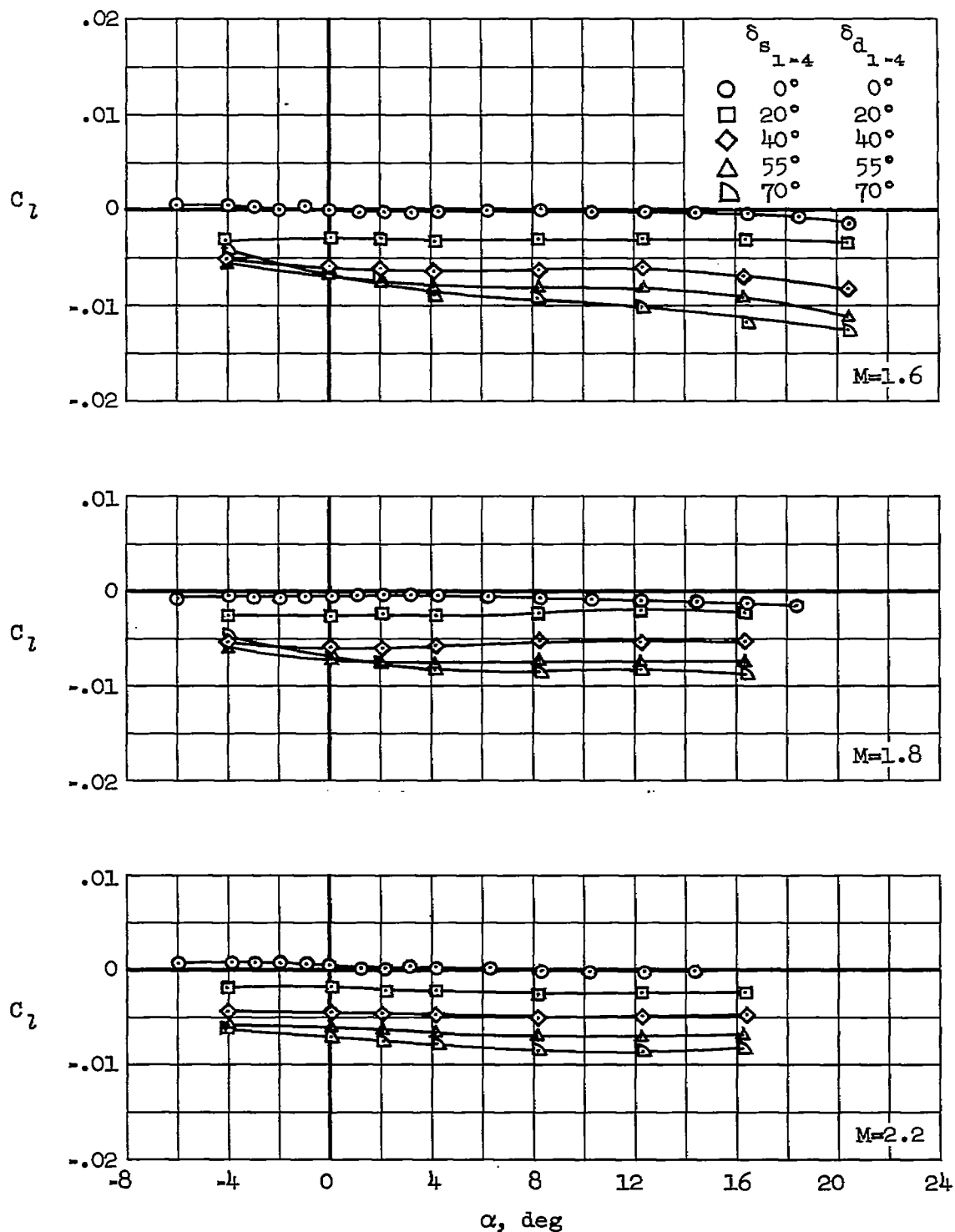
~~CONFIDENTIAL~~

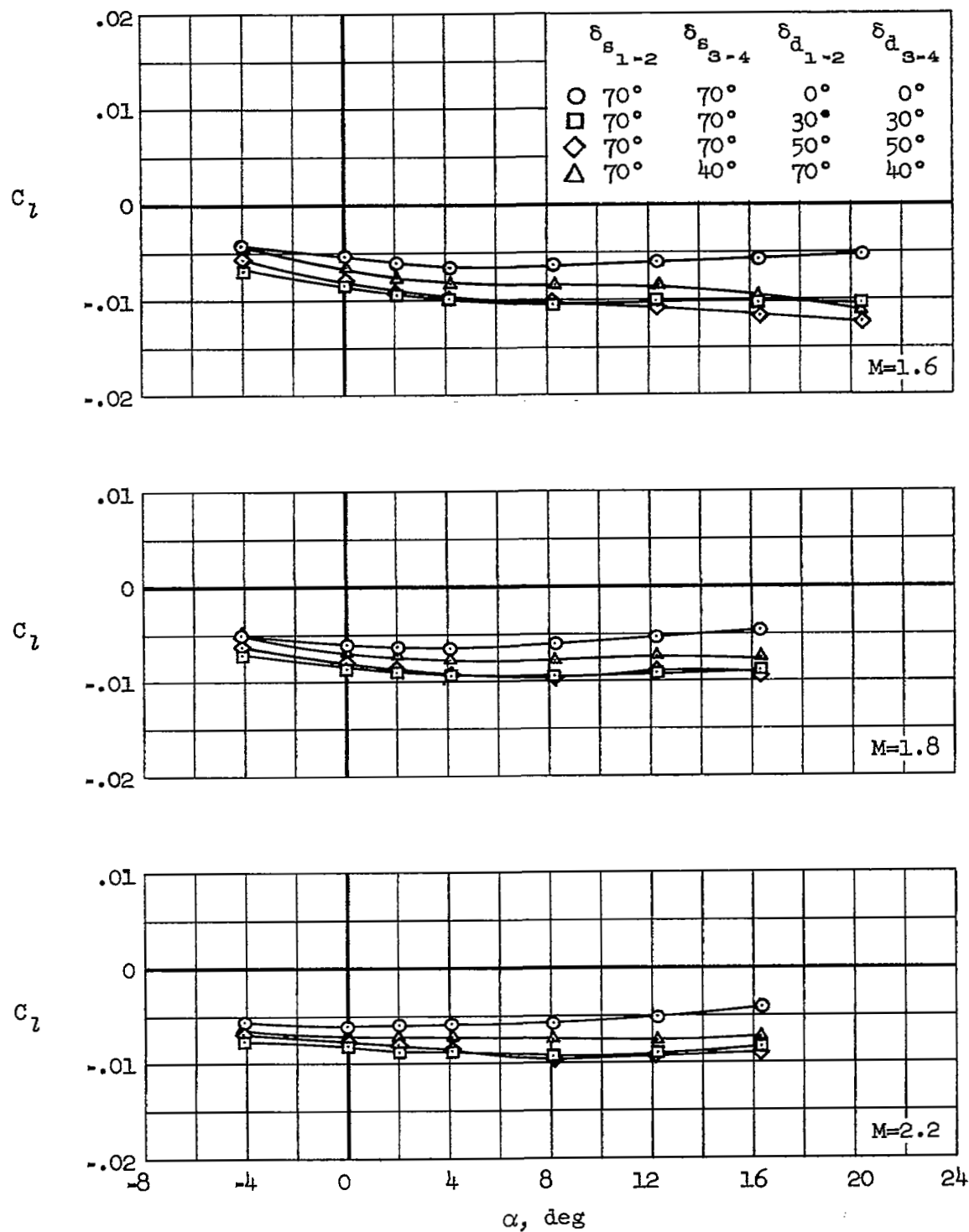
Figure 14.- Concluded.

~~CONFIDENTIAL~~



(a) Equal spoiler and deflector angles.

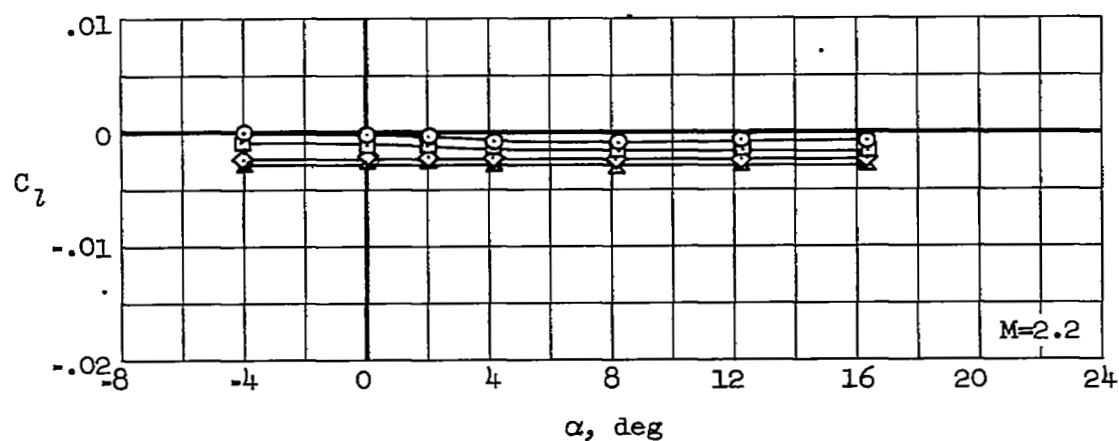
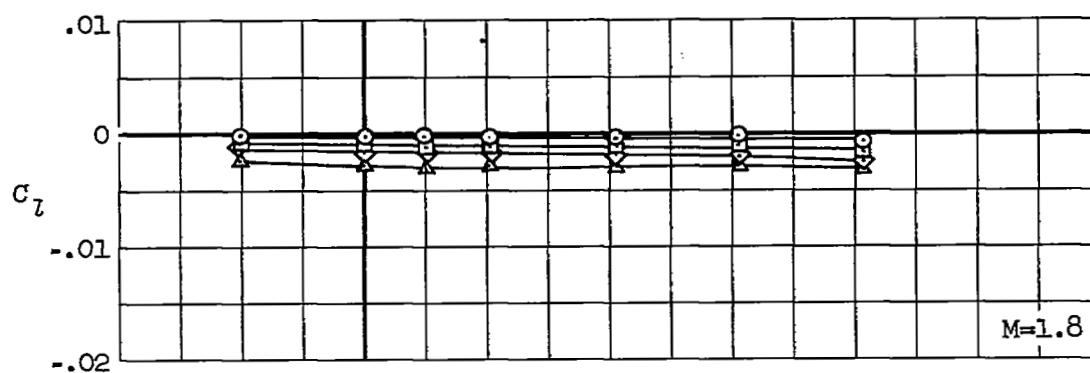
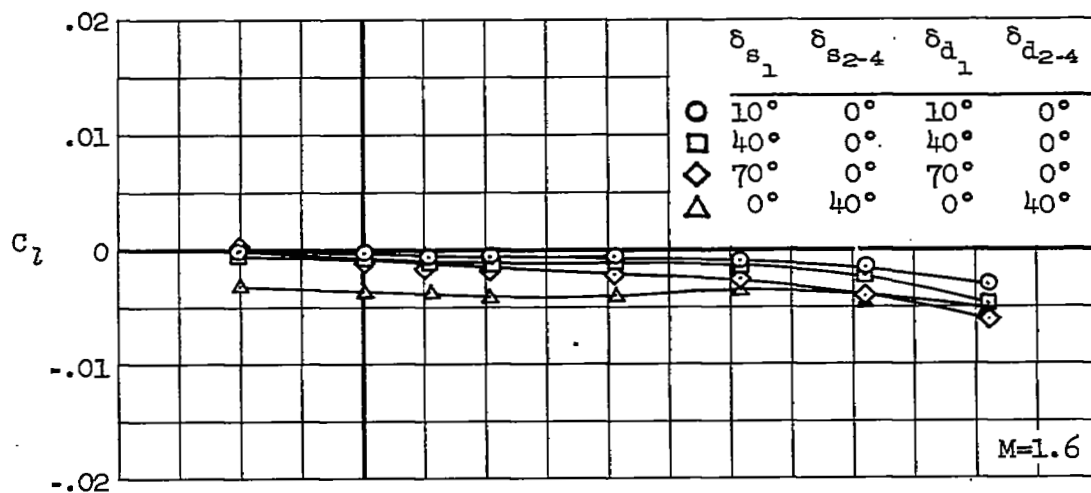
Figure 15.- Rolling-moment effects of spoiler deflection for basic configuration.



(b) Various deflector angles.

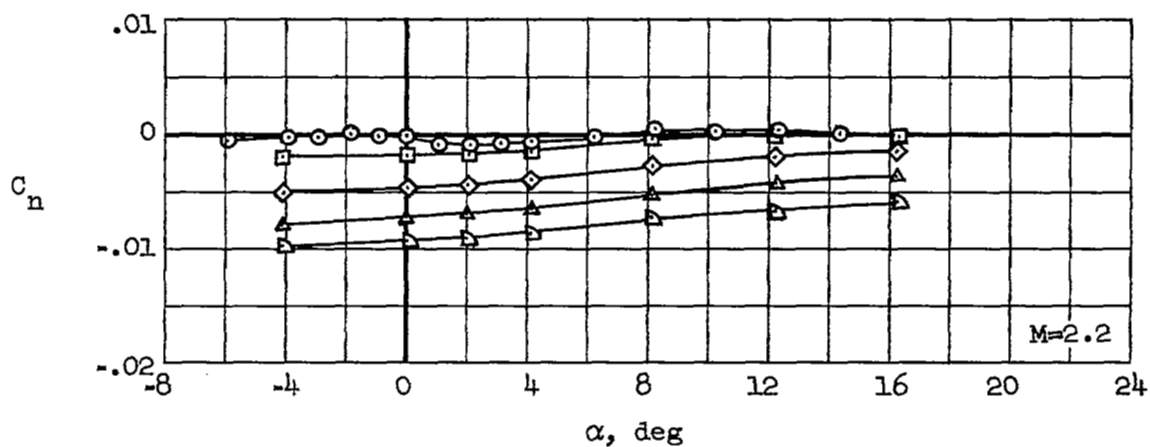
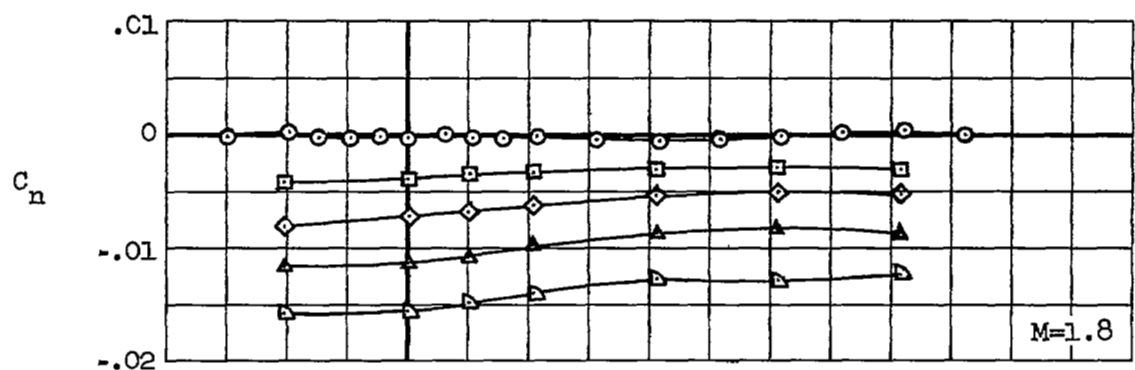
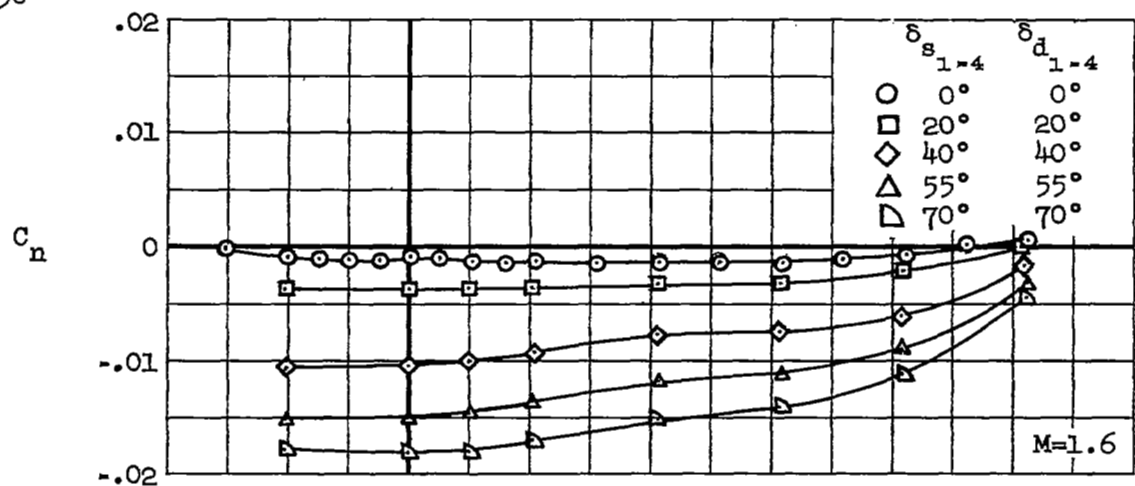
Figure 15.- Continued.

~~CONFIDENTIAL~~



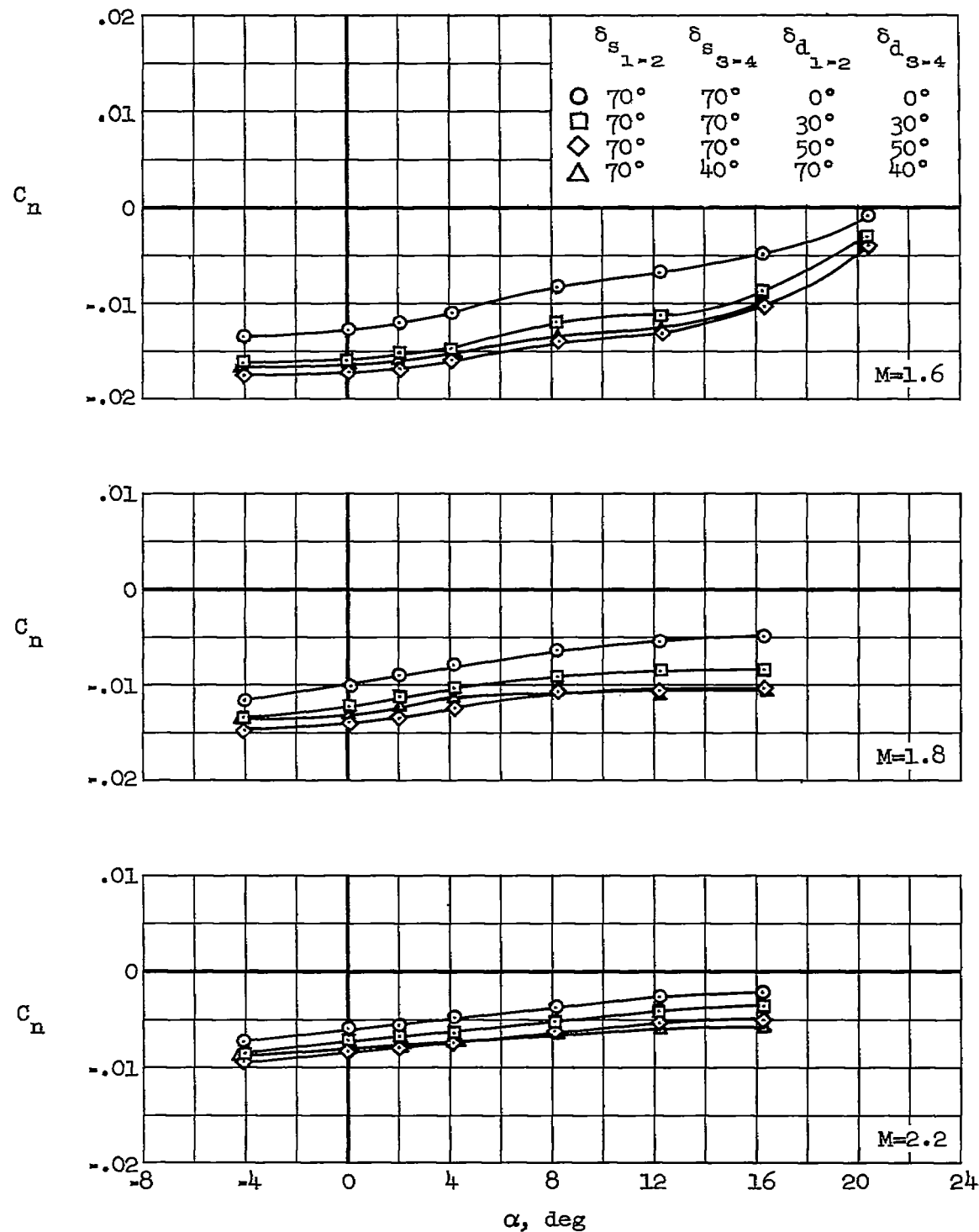
(c) Inboard spoiler and deflector only.

Figure 15.- Concluded.



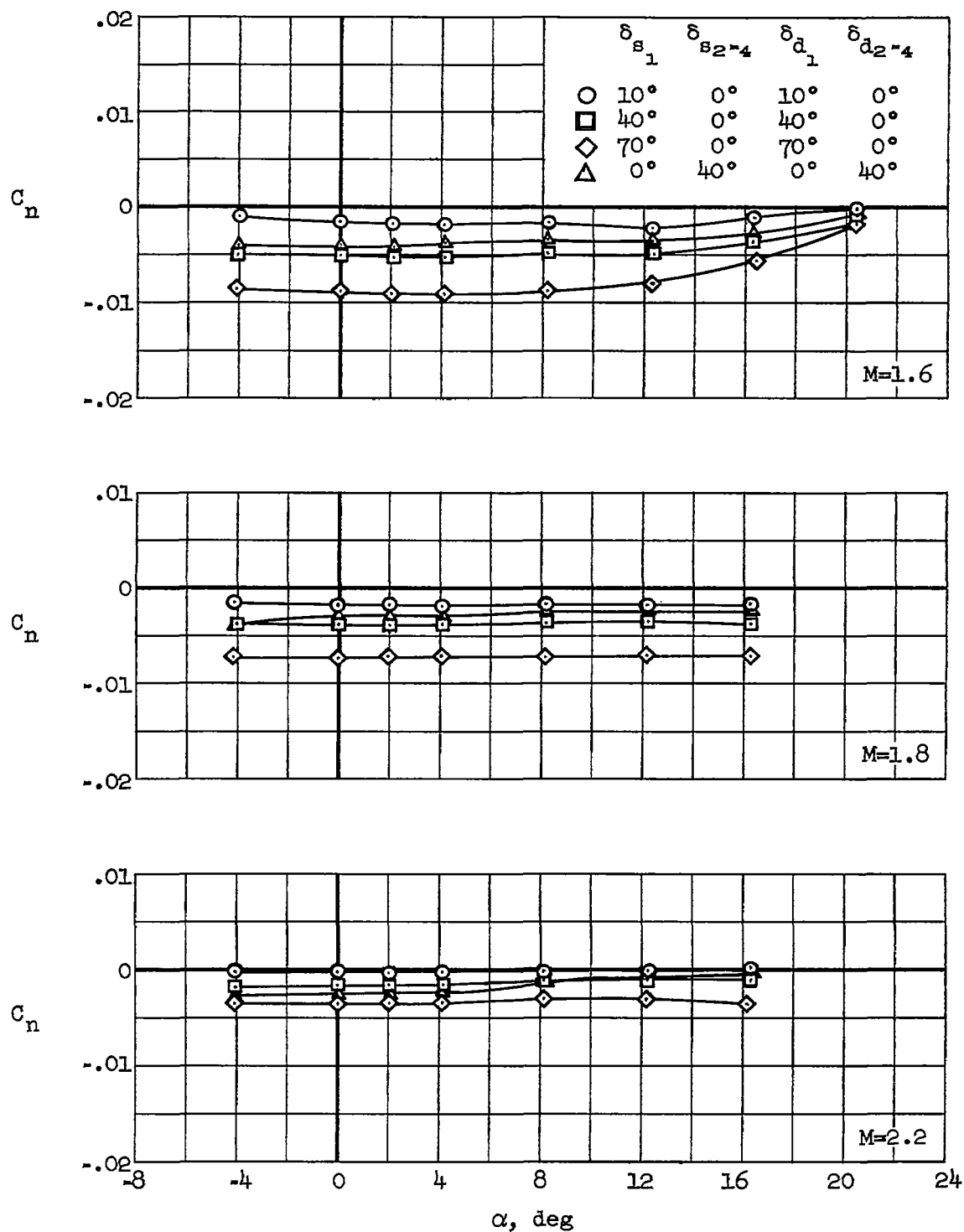
(a) Equal spoiler and deflector angles.

Figure 16.- Yawing-moment effects of spoiler deflection for basic



(b) Various deflector angles.

Figure 16.- Continued.



(c) Inboard spoiler and deflector only.

Figure 16.- Concluded.

~~CONFIDENTIAL~~

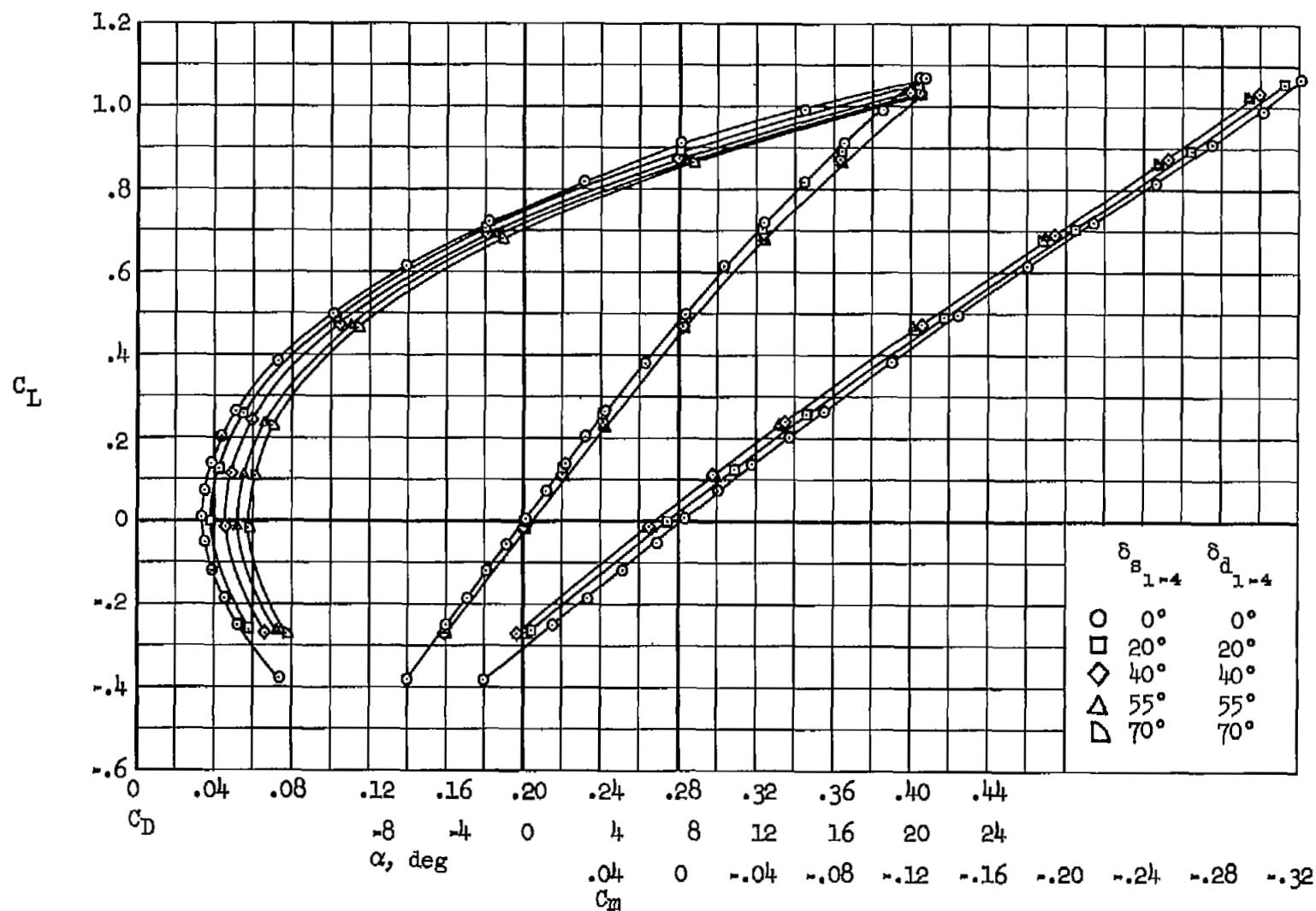
(a) $M = 1.6$

Figure 17.- Effect of spoiler deflection on longitudinal characteristics of the basic configuration.

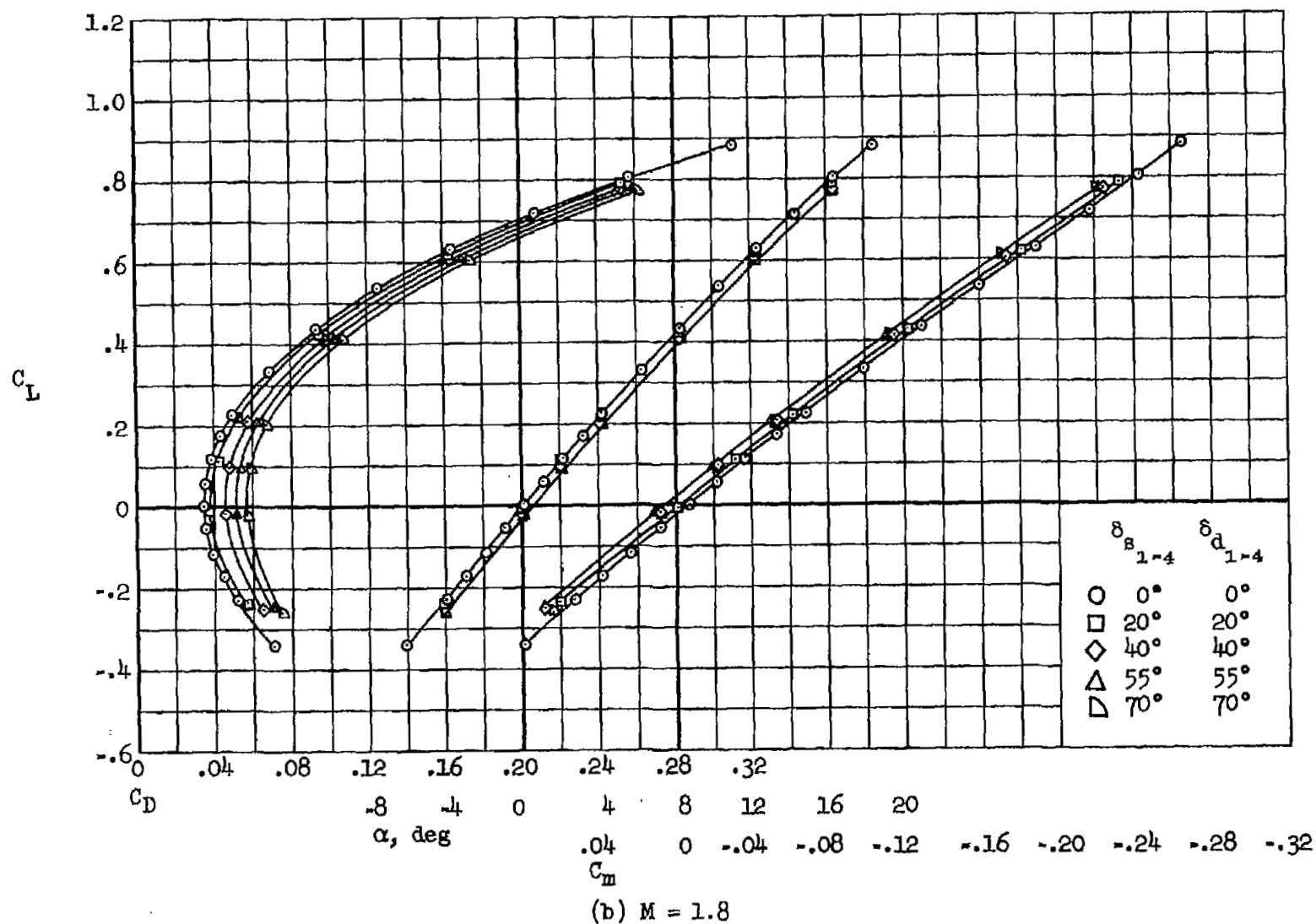
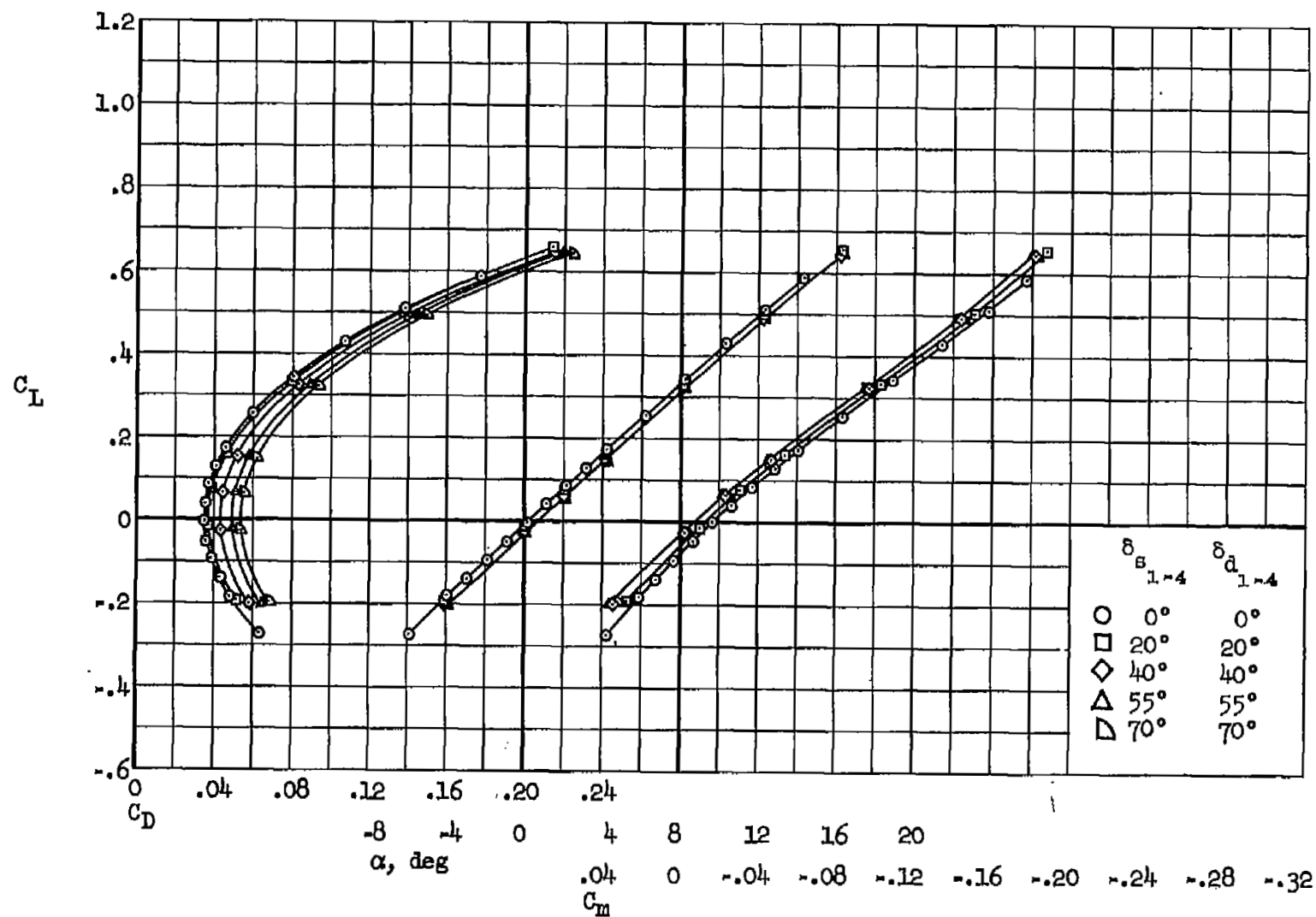


Figure 17.- Continued.



(c) $M = 2.2$

Figure 17.- Concluded.

NASA Technical Library



3 1176 01434 9501

CONFIDENTIAL